From species diffusion to poroelasticity and the modeling of lamina cribrosa

A. Tatone[a,*], F. Recrosi[b], R. Repetto[c], G. Guidoboni[d]

[a]*DISIM, Università dell'Aquila, L'Aquila, Italy*
[b]*GSSI, L'Aquila, Italy*
[c]*DICCA, Università di Genova, Genova, Italy*
[d]*College of Engineering, University of Missouri, Columbia, Mo, USA*

Abstract

The Lamina Cribrosa is a part of the optic nerve head acting as a scaffold for collecting the retinal ganglion cell axons. It can be modeled as a poroelastic material where the saturated porosity stands for the capillary network running inside the collagen beams. Our aim is to study the interaction between tissue porosity, deformation and hemodynamics. To this end we first focus on the derivation of a poroelastic model in a rather general case, using as a prototype a model of species diffusion in an elastic material. Then we outline the clinical significance of the mechanical behavior of the Lamina Cribrosa and show, through numerical simulations, how an increased intraocular pressure results in a deformation affecting porosity and blood perfusion. We emphasize how the model behavior relies on the free energy expression.

Keywords: diffusion, poroelasticity, soft tissues, hemodynamics, glaucoma, lamina cribrosa

Contents

*Corresponding author
Email addresses:* `amabile.tatone@univaq.it` (A. Tatone), `filippo.recrosi@gssi.infn.it` (F. Recrosi),
`rodolfo.repetto@unige.it` (R. Repetto), `guidobonig@missouri.edu` (G. Guidoboni)

1. Introduction

An increased pressure inside the vitreous chamber (intraocular pressure, IOP) is a major risk factor for optic nerve damage. The optic nerve carries, through the axons, signals generated by the retina to the brain. A damaged optic nerve results in vision impairment and blindness (glaucoma) [1].

The Lamina Cribrosa (LC) is a laminar region, part of the optic nerve head (ONH), made up of a fenestrated meshwork of thin collagen beams acting as a scaffold for collecting the retinal ganglion cell (RGC) axons, grouped in bundles [2]. It is also the region crucial to blood supply and drainage. Ganglion cell axons and surrounding glial elements are dependent on the local blood supply for their energy requirements [3]. Other biological functions of the LC are in sustaining the central retina vein (CRV) and central retinal artery (CRA), passing through the optic nerve towards the retina, and in stabilizing the pressure difference between IOP and the retrolaminar tissue pressure (RLTp).

The main blood supply to the optic nerve head is from the posterior ciliary artery via the peripapillary choroid and short posterior ciliary arteries (the circle of Zinn-Haller). Raised IOP may result in an alteration of the blood supply to the optic nerve head to induce ischemia [3].

Even though the pathogenesis of glaucoma is far from being understood, we know that mechanics plays a key role in its onset and development [4, 5, 6, 7]. A comprehensive overview of the many factors which can be related to

glaucoma is summarized in a diagram in [8, Fig. 2], where we can find: *tissue deformation*, *stress and strain*, altered *blood flow* and *nutrient supply*. Hemodynamic alterations in the lamina cribrosa have also been identified in [9] as strongly related to glaucoma. In [10] it is emphasized how a deformation of the structurally weak LC due to large IOP values can lead to an impairment of axonal transport and blood flow.

In the computational modeling in [11] the LC is described as a framework made up of connected thin hollow cylinders. Hemodynamics and oxygen diffusion are then statistically characterized by morphologic factors through a large number of simulations.

In our work, we aim at combining the mechanical and hemodynamic viewpoints and study the interaction between deformation and blood perfusion in a continuum. We model the lamina cribrosa as a poroelastic soft material where a saturated porosity network stands for the capillary network running inside the collagen beams [12].

To this end we first focus on the derivation of a poroelastic model in a rather general case, using as a prototype the model of species diffusion in an elastic material. This task is carried out by transforming, in a natural way, quantities appropriate to a diffusing species, like *concentration*, *chemical potential* and *molar flux* into the corresponding quantities which are appropriate to a saturated porous material, like *porosity*, *interstitial pressure* and *discharge*, while retaining the usual description for a nonlinear elastic solid, based on *deformation* and *stress*. We get a couple of *power balance laws*, for both the forces and the amount of fluid filling the porosity network, in such a way that it is natural to state an *energy imbalance principle* from which we draw a constitutive characterization coupling deformation and stress with porosity, and leading to Darcy's law as well. We emphasize how this characterization relies on the expression for the *free energy*, in particular on the way it depends on porosity.

The power balance laws allows us to state clearly the basic boundary conditions and to illustrate their meaning. In particular, by *permeable boundary* we mean a condition where the interstitial pressure in a thin boundary layer equals the external pressure.

Further we show how to derive a suitable description of a porosity dependent *permeability* in the LC, based on a simple microscopic model of the capillary network. Then we describe some numerical simulations we conducted on a thick small spherical cap, approximately the same shape and size as the Lamina Cribrosa, cast in the peripapillary sclera, which show how an increased IOP results in a deformation leading to a non uniform porosity and a reduced blood flow.

2. Species diffusion in a crystal lattice

The charging process of a Lithium battery has recently drawn much interest [13, 14, 15] for its industrial relevance. It consists mainly in the diffusion of Lithium atoms in a Silicon anode. We look at this process as an exemplary case of atomic diffusion in a crystal lattice [16] and outline here the basic *chemo-mechanical* setting, denoting by "b" the diffusing species. This setting will be used later as a prototype for deriving a model of fluid perfusion in an elastic material.
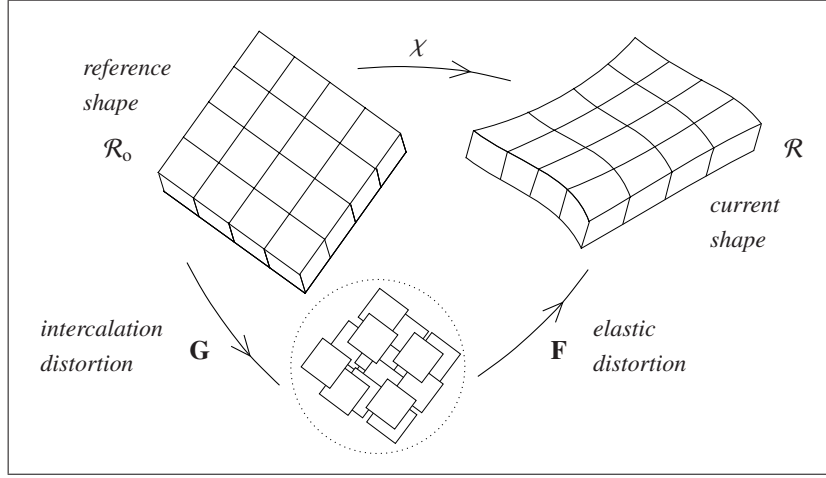
Figure 1: Decomposition of the deformation gradient $\nabla\chi$.

2.1. Kinematics and kinetics

Let us denote by

$$\chi : \mathcal{R}_\mathrm{o} \to \mathcal{R}, \tag{1}$$

a time dependent deformation of a crystal lattice from the reference shape to the current shape. Describing the *intercalation distortion* of a crystal lattice [17] as a spherical tensor field

$$\mathbf{G} = \beta^{\frac{1}{3}}\,\mathbf{I}, \tag{2}$$

with $\det \mathbf{G} = \beta$, and ruling out any plastic distortion, the accompanying *elastic distortion* $\mathbf{F}$ is defined by the deformation gradient decomposition

$$\mathbf{F}_\mathrm{o} \equiv \nabla\chi = \mathbf{F}\,\mathbf{G}, \tag{3}$$

which is illustrated by the schematic diagram in Fig. 1. It is convenient to describe the amount of intercalated ♭-atoms by the *concentration*

$$c = \frac{\rho_\flat}{\rho_\mathrm{o}} = \frac{<\text{molar density of species } \flat \text{ per unit reference volume}>}{<\text{molar density of lattice sites per unit reference volume}>}, \tag{4}$$

and make the assumption that it is related to the lattice volume change through

$$\beta = 1 + \alpha\,(c - c_\mathrm{o}), \tag{5}$$

where α is a stoichiometric positive constant coefficient and c_o is a reference concentration.

If we denote by ρ the molar density of lattice sites *per unit current volume*, then for any regular subset $\mathcal{P} \subset \mathcal{R}$ which is *convected* from a reference subset $\mathcal{P}_\mathrm{o} \subset \mathcal{R}_\mathrm{o}$ by the same deformation (1)

$$\chi : \mathcal{P}_\mathrm{o} \to \mathcal{P}, \tag{6}$$

4

the *molar conservation law* of lattice sites reads[1]

$$0 = \frac{d}{dt} \int_{\mathcal{P}} \rho \, dV = \frac{d}{dt} \int_{\mathcal{P}_\mathrm{o}} \rho \, \det \mathbf{F}_\mathrm{o} \, dV = \int_{\mathcal{P}_\mathrm{o}} (\dot{\rho} + \rho \, \mathrm{tr} \, \nabla \mathbf{v}) \det \mathbf{F}_\mathrm{o} \, dV , \qquad (7)$$

and localizes to

$$\dot{\rho} + \rho \, \mathrm{div} \, \mathbf{v} = 0 . \qquad (8)$$

Since by definition (4) the product $c\rho$ is the molar density of species $\flat$ per unit current volume, the rate of change of the amount of species $\flat$ will be instead

$$\frac{d}{dt} \int_{\mathcal{P}} c\rho \, dV = \frac{d}{dt} \int_{\mathcal{P}_\mathrm{o}} c\rho \, \det \mathbf{F}_\mathrm{o} \, dV = \frac{d}{dt} \int_{\mathcal{P}_\mathrm{o}} c\rho_\mathrm{o} \, dV = \int_{\mathcal{P}_\mathrm{o}} \dot{c}\rho_\mathrm{o} \, dV = \int_{\mathcal{P}} \dot{c}\rho \, dV . \qquad (9)$$

2.2. From the species molar balance to the species power balance

Denoting by $\mathbf{h}$ the *molar flux* per unit current area, and by h a *supply* density per unit current volume, the species $\flat$ *molar balance law* reads

$$\int_{\mathcal{P}} \dot{c}\rho \, dV = - \int_{\partial\mathcal{P}} \mathbf{h} \cdot \mathbf{n} \, dA + \int_{\mathcal{P}} h \, dV , \qquad (10)$$

and localizes to

$$\dot{c}\rho = - \mathrm{div} \, \mathbf{h} + h , \qquad (11)$$

from which we will drop the supply term, thus assuming $h = 0$.

Let us set now a scalar field $\underline{\mu}$, power conjugate to the kinetic descriptor $\dot{c}\rho$, transforming the *molar balance law* (11) into a *power balance law*

$$\int_{\mathcal{P}} \underline{\mu} \, \dot{c}\rho \, dV = - \int_{\mathcal{P}} \underline{\mu} \, \mathrm{div} \, \mathbf{h} \, dV \qquad \forall \underline{\mu} . \qquad (12)$$

Since

$$\mathrm{div}(\mu \, \mathbf{h}) = \mu \, \mathrm{div} \, \mathbf{h} + \mathbf{h} \cdot \nabla \mu , \qquad (13)$$

we get finally the *molar balance law* (10) replaced by the *power balance law*

$$\int_{\mathcal{P}} \underline{\mu} \, \dot{c}\rho \, dV = - \int_{\partial\mathcal{P}} \underline{\mu} \, \mathbf{h} \cdot \mathbf{n} \, dA + \int_{\mathcal{P}} \mathbf{h} \cdot \nabla\underline{\mu} \, dV \qquad \forall \underline{\mu} . \qquad (14)$$

Notice that $\underline{\mu}$ (*energy per mole*) is a *chemical potential*, acting here just as a test field.[2]

Finally it is worth noting that although equation (14) can be interpreted as the balance of an *energy transport*, its derivation differs from the corresponding one in [16].

---

[1] A superposed dot will denote time derivative.

[2] Throughout the paper we will consistently denote *test* fields by underlying the corresponding symbol.

2.3. Power balance laws

We can move the species power balance (14) back to the reference shape, and get $\forall \mathcal{P}_o \subset \mathcal{R}_o$

$$\int_{\mathcal{P}_o} \mu \, \dot{c} \, \rho_o \, dV = -\int_{\partial \mathcal{P}_o} \mu \, \mathbf{h}_o \cdot \mathbf{n}_o \, dA + \int_{\mathcal{P}_o} \mathbf{h}_o \cdot \nabla_o \mu \, dV \qquad \forall \underline{\mu}, \tag{15}$$

using first the identity relating the reference and the current gradient of the scalar field μ, which we get from

$$\forall \mathbf{e} \quad (\nabla_o \mu) \cdot \mathbf{e} = (\nabla \mu) \cdot \mathbf{F}_o \, \mathbf{e} \quad \Rightarrow \quad \nabla_o \mu = \mathbf{F}_o^\mathsf{T} \, \nabla \mu, \tag{16}$$

then replacing the current flux with the reference flux, according to the relation

$$\mathbf{h}_o = (\det \mathbf{F}_o) \, \mathbf{F}_o^{-1} \, \mathbf{h}, \tag{17}$$

derived by the following surface integral transform

$$\int_{\partial \mathcal{P}} \mu \, \mathbf{h} \cdot \mathbf{n} \, dA = \int_{\partial \mathcal{P}_o} \mu \, \mathbf{h} \cdot ((\det \mathbf{F}_o) \, \mathbf{F}_o^{-\mathsf{T}} \, \mathbf{n}_o) \, dA = \int_{\partial \mathcal{P}_o} \mu \, \mathbf{h}_o \cdot \mathbf{n}_o \, dA. \tag{18}$$

Since we are interested in coupling species diffusion to deformation and stress we state now the *force power balance law*, $\forall \mathcal{P}_o \subset \mathcal{R}_o$,

$$\int_{\mathcal{P}_o} \mathbf{b}_o \cdot \underline{\mathbf{v}} \, dV + \int_{\partial \mathcal{P}_o} \mathbf{t}_o \cdot \underline{\mathbf{v}} \, dA = \int_{\mathcal{P}_o} \mathbf{S}_o \cdot \nabla_o \underline{\mathbf{v}} \, dV \qquad \forall \underline{\mathbf{v}}, \tag{19}$$

where $\mathbf{b}_o$ and $\mathbf{t}_o$ stand for the reference bulk force density and the reference boundary traction. The reference Piola stress $\mathbf{S}_o$, the Cauchy stress $\mathbf{T}$ and the intermediate Piola stress $\mathbf{S}$ turn out to be related one another by

$$\mathbf{S}_o = (\det \mathbf{F}_o) \, \mathbf{T} \, \mathbf{F}_o^{-\mathsf{T}} = \beta (\det \mathbf{F}) \, \mathbf{T} \, \mathbf{F}_o^{-\mathsf{T}} = \beta^{\frac{2}{3}} (\det \mathbf{F}) \, \mathbf{T} \, \mathbf{F}^{-\mathsf{T}} = \beta^{\frac{2}{3}} \, \mathbf{S}, \tag{20}$$

according to the following volume integral transform

$$\int_{\mathcal{P}} \mathbf{T} \cdot \nabla \mathbf{v} \, dV = \int_{\mathcal{P}_o} (\det \mathbf{F}_o) \mathbf{T} \, \mathbf{F}_o^{-\mathsf{T}} \cdot \nabla_o \mathbf{v} \, dV = \int_{\mathcal{P}_o} \mathbf{S}_o \cdot \nabla_o \mathbf{v} \, dV, \tag{21}$$

where the current gradient of the vector field $\mathbf{v}$ is related to the reference one by the identity we get from

$$\forall \mathbf{e} \quad (\nabla_o \mathbf{v}) \, \mathbf{e} = (\nabla \mathbf{v}) \, \mathbf{F}_o \, \mathbf{e} \quad \Rightarrow \quad \nabla_o \mathbf{v} = (\nabla \mathbf{v}) \, \mathbf{F}_o. \tag{22}$$

The standard *frame-invariance* argument, stating that $\mathbf{T} \cdot \nabla \underline{\mathbf{v}} = 0$ for any rigid test velocity field, leads to the symmetry property of tensor $\mathbf{T}$.

2.4. Free energy imbalance

Let us consider now any evolution of the model we are defining, i.e. any *constitutive process*, and the corresponding force power balance

$$\underbrace{\int_{\mathcal{P}_o} \mathbf{b}_o \cdot \mathbf{v} \, dV + \int_{\partial \mathcal{P}_o} \mathbf{t}_o \cdot \mathbf{v} \, dA}_{\textit{(exchanged) external power}} = \int_{\mathcal{P}_o} \mathbf{S}_o \cdot \dot{\mathbf{F}}_o \, dV, \tag{23}$$

together with the species power balance

$$\int_{\mathcal{P}_o} \mu \, \dot{c} \, \rho_o \, dV = \underbrace{- \int_{\partial \mathcal{P}_o} \mu \, \mathbf{h}_o \cdot \mathbf{n}_o \, dA}_{\text{(exchanged) external power}} + \int_{\mathcal{P}_o} \mathbf{h}_o \cdot \nabla_o \mu \, dV \,. \tag{24}$$

Comparing the power exchanged between the matter inside any $\mathcal{P}_o$ and the outside with the rate of change of a free energy density per unit reference volume ψ, we state the *energy imbalance* or *dissipation inequality* [16, 18]

$$\mathbf{S}_o \cdot \dot{\mathbf{F}}_o + \mu \, \rho_o \, \dot{c} - \mathbf{h}_o \cdot \nabla_o \mu - \frac{d}{dt} \psi \geq 0 \,. \tag{25}$$

By (20), (3) and (5), the stress power term in (25) can be given the expression

$$\mathbf{S}_o \cdot \dot{\mathbf{F}}_o = \beta \, \mathbf{S} \cdot \dot{\mathbf{F}} + \frac{1}{3} \mathbf{S} \cdot \mathbf{F} \, \alpha \, \dot{c} \,, \tag{26}$$

which, since

$$\mathbf{S} \cdot \mathbf{F} = (\det \mathbf{F}) \, \mathbf{T} \, \mathbf{F}^{-\mathsf{T}} \cdot \mathbf{F} = (\det \mathbf{F}) \, \mathbf{T} \cdot \mathbf{I} = (\det \mathbf{F}) \, \mathrm{tr} \, \mathbf{T} \,, \tag{27}$$

simplifies to

$$\mathbf{S}_o \cdot \dot{\mathbf{F}}_o = \beta \, \mathbf{S} \cdot \dot{\mathbf{F}} - J \, p \, \alpha \, \dot{c} \,, \tag{28}$$

with

$$J := \det \mathbf{F} \,, \quad p := -\frac{1}{3} \, \mathrm{tr} \, \mathbf{T} \,. \tag{29}$$

Therefore the inequality (25) can be rewritten as

$$\beta \, \mathbf{S} \cdot \dot{\mathbf{F}} + (\mu \, \rho_o - J \, p \, \alpha) \, \dot{c} - \mathbf{h}_o \cdot \nabla_o \mu - \frac{d}{dt} \psi \geq 0 \,. \tag{30}$$

2.5. Free energy expression and constitutive characterization

Looking at (30) let us choose a free energy expression like the one given in [13, 14, 19]

$$\psi = \hat{\psi}(\mathbf{F}, c) = \varphi_{ch}(c) + \beta \, \varphi_e(\mathbf{F}) \,, \tag{31}$$

which is the sum of a *chemical energy* density per unit reference volume, and a *strain energy* density per unit intermediate volume. Defining the response functions $\hat{\mu}_{ch}$ and $\hat{\mathbf{S}}$ such that

$$\rho_o \, \hat{\mu}_{ch}(c) \, \dot{c} = \frac{d}{dt} \varphi_{ch}(c) \,, \tag{32}$$

$$\hat{\mathbf{S}}(\mathbf{F}) \cdot \dot{\mathbf{F}} = \frac{d}{dt} \varphi_e(\mathbf{F}) \,, \tag{33}$$

the rate of change of the free energy, because of the decomposition (3) and the assumption (5), turns out to be

$$\frac{d}{dt} \hat{\psi}(\mathbf{F}, c) = \beta \, \hat{\mathbf{S}}(\mathbf{F}) \cdot \dot{\mathbf{F}} + (\alpha \, \varphi_e(\mathbf{F}) + \rho_o \, \hat{\mu}_{ch}(c)) \, \dot{c} \,. \tag{34}$$

7

If we finally substitute (34) into (30) we get

$$\beta \, (\underbrace{\mathbf{S} - \hat{\mathbf{S}}(\mathbf{F})}_{\mathbf{S}^+}) \cdot \dot{\mathbf{F}} + (\underbrace{\rho_{\mathrm{o}} \, (\mu - \hat{\mu}_{ch}(c)) - \alpha \, (J \, p + \varphi_e(\mathbf{F}))}_{\rho_{\mathrm{o}} \, \mu^+}) \, \dot{c} - \mathbf{h}_{\mathrm{o}} \cdot \nabla_{\mathrm{o}} \mu \geq 0 \,. \tag{35}$$

In order for the inequality (35) to hold for any constitutive process the following conditions must be fulfilled

$$\mu = \hat{\mu}_{ch}(c) + \frac{\alpha}{\rho_{\mathrm{o}}} (J \, p + \varphi_e(\mathbf{F})) + \mu^+ \,, \quad \mu^+ \dot{c} \geq 0 \,, \tag{36}$$

$$\mathbf{S} = \hat{\mathbf{S}}(\mathbf{F}) + \mathbf{S}^+ \,, \quad \mathbf{S}^+ \cdot \dot{\mathbf{F}} \geq 0 \,, \tag{37}$$

$$-\mathbf{h}_{\mathrm{o}} \cdot \nabla_{\mathrm{o}} \mu \geq 0 \,, \tag{38}$$

with $\mathbf{S}^+$ and μ^+ possibly describing dissipative mechanisms.

Notice how the coupling between diffusion and stress is described by the expression (36) characterizing the chemical potential through the spherical part of the Eshelby tensor [20, 19]

$$\mathbf{E} = -\mathbf{F}^{\mathsf{T}} \mathbf{S} + \varphi_e(\mathbf{F}) \, \mathbf{I} \,. \tag{39}$$

2.6. Fick's law

The last condition (38) holds true if

$$\mathbf{h}_{\mathrm{o}} = -\mathbf{M}_{\mathrm{o}} \, \nabla_{\mathrm{o}} \mu \,, \tag{40}$$

with $\mathbf{M}_{\mathrm{o}}$ a positive semi-definite tensor. Expression (40) is the reference form of *Fick's law*. By (16) and (17) the reference flux and the reference chemical potential gradient can be transformed into the corresponding current quantities, leading to the new expression of *Fick's law*

$$\mathbf{h} = -\mathbf{M} \, \nabla \mu \,, \tag{41}$$

where the reference and the current *mobility* tensors are related by

$$\mathbf{M}_{\mathrm{o}} = \beta \, (\det \mathbf{F}) \, \mathbf{F}_{\mathrm{o}}^{-1} \, \mathbf{M} \, \mathbf{F}_{\mathrm{o}}^{-\mathsf{T}} \tag{42}$$

2.7. Strain energy splitting

Let us assume that the strain energy can be decomposed as

$$\varphi_e(\mathbf{F}) = \varphi_\iota(\mathbf{F}_\iota) + \varphi_{vol}(J) \,, \tag{43}$$

where $\mathbf{F}_\iota$ is the *isochoric* part of the elastic distortion $\mathbf{F}$ defined by

$$\mathbf{F} = J^{\frac{1}{3}} \, \mathbf{F}_\iota \,. \tag{44}$$

8

The corresponding velocity gradient decomposition

$$\dot{\mathbf{F}}\,\mathbf{F}^{-1} = \dot{\mathbf{F}}_\iota\,\mathbf{F}_\iota^{-1} + \frac{1}{3}\,\mathbf{I}\,\dot{J}/J \tag{45}$$

leads to

$$\mathbf{S}\cdot\dot{\mathbf{F}} = J\,\mathbf{T}\cdot\dot{\mathbf{F}}\,\mathbf{F}^{-1} = J\,\mathbf{T}\cdot\dot{\mathbf{F}}_\iota\,\mathbf{F}_\iota^{-1} + \frac{1}{3}\mathbf{T}\cdot\mathbf{I}\,\dot{J} = J\,\mathrm{dev}\,\mathbf{T}\cdot\dot{\mathbf{F}}_\iota\,\mathbf{F}_\iota^{-1} + \frac{1}{3}\,\mathrm{tr}\,\mathbf{T}\,\dot{J}\,, \tag{46}$$

as well as

$$\hat{\mathbf{S}}(\mathbf{F})\cdot\dot{\mathbf{F}} = J\,\mathrm{dev}\,\hat{\mathbf{T}}(\mathbf{F})\cdot\dot{\mathbf{F}}_\iota\,\mathbf{F}_\iota^{-1} + \frac{1}{3}\,\mathrm{tr}\,\hat{\mathbf{T}}(\mathbf{F})\,\dot{J}\,. \tag{47}$$

Denoting by

$$\mathbf{S}_\iota = (\mathrm{dev}\,\mathbf{T})\,\mathbf{F}_\iota^\mathsf{T}\,, \tag{48}$$

and, consistently with the definition of p in (29),

$$\hat{\mathbf{S}}_\iota(\mathbf{F}) = (\mathrm{dev}\,\hat{\mathbf{T}}(\mathbf{F}))\,\mathbf{F}_\iota^\mathsf{T}\,,$$

$$\hat{p}_e(\mathbf{F}) = -\frac{1}{3}\,\mathrm{tr}\,\hat{\mathbf{T}}(\mathbf{F})\,, \tag{49}$$

the expressions (46) and (47) simplify to

$$\mathbf{S}\cdot\dot{\mathbf{F}} = J\,\mathbf{S}_\iota\cdot\dot{\mathbf{F}}_\iota - p\,\dot{J}\,, \tag{50}$$

$$\hat{\mathbf{S}}(\mathbf{F})\cdot\dot{\mathbf{F}} = J\,\hat{\mathbf{S}}_\iota(\mathbf{F})\cdot\dot{\mathbf{F}}_\iota - \hat{p}_e(\mathbf{F})\,\dot{J}\,. \tag{51}$$

Replacing (50) and (51) respectively into (26) and (34), the dissipation inequality (30) leads to the new form of (35)

$$\beta\,J\,\big(\underbrace{\mathbf{S}_\iota - \hat{\mathbf{S}}_\iota(\mathbf{F})}_{\mathbf{S}_\iota^+}\big)\cdot\dot{\mathbf{F}}_\iota - \big(\underbrace{p - \hat{p}_e(\mathbf{F})}_{p^+}\big)\beta\,\dot{J} + \big(\underbrace{\rho_\mathrm{o}\,(\mu - \hat{\mu}_{ch}(c)) - \alpha\,(J\,p + \varphi_e(\mathbf{F}))}_{\rho_\mathrm{o}\,\mu^+}\big)\dot{c} - \mathbf{h}_\mathrm{o}\cdot\nabla_\mathrm{o}\mu \geq 0\,, \tag{52}$$

from which we get a more detailed constitutive characterization for the stress

$$\mathbf{S}_\iota = \hat{\mathbf{S}}_\iota(\mathbf{F}) + \mathbf{S}_\iota^+\,, \quad \mathbf{S}_\iota^+\cdot\dot{\mathbf{F}}_\iota \geq 0\,, \tag{53}$$

$$p = \hat{p}_e(\mathbf{F}) + p^+\,, \quad -p^+\cdot\dot{J} \geq 0\,, \tag{54}$$

with $\mathbf{S}_\iota^+$ and p^+ possibly describing different dissipative mechanisms, while (36) and (38) still hold unchanged.

3. From species diffusion to poroelasticity

From the diffusion of a single species in an elastic solid, described in the previous section, we now derive a model for the perfusion of a fluid, by assuming that the fluid is incompressible and flows through a porosity network which it keeps saturated. This way we recover a poroelasticity theory as a special case of a diffusion theory where the species concentration has been replaced by the saturated porosity.
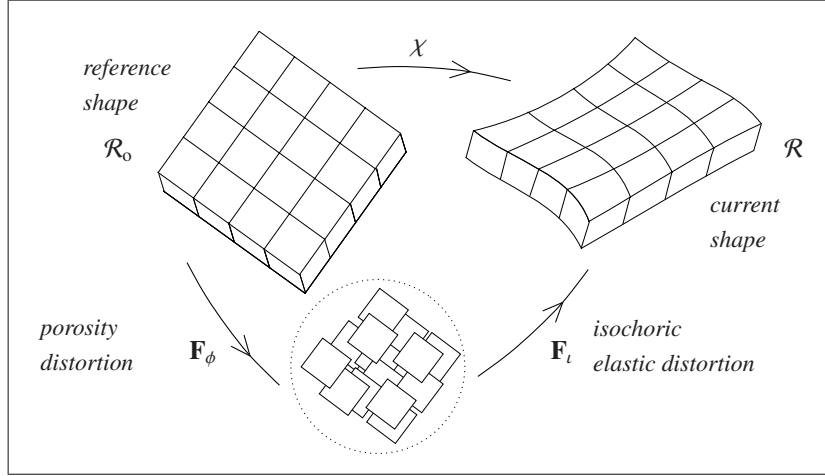
9

Figure 2: Decomposition of the deformation gradient $\nabla \chi$.

Our aim is just to lay down a self-contained, neat and consistent framework, suitable for our modeling purposes and numerical simulations. We cared about consistency of our setting with the relevant scientific literature, from the classical work [21] to the historical description [22] or the comprehensive book [23], as well as works on the many variants of poroelasticity [24, 25, 26], including polymeric gels [27, 28, 29] and blood perfusion [30]. Nevertheless no explicit detailed references will in general be made neither to basic relations nor to main results therein.

3.1. Deformation and porosity

Let us denote by $\chi : \mathcal{R}_o \rightarrow \mathcal{R}$, as in (1), a time dependent deformation of a body made up of a porous material whose pores are filled at any time with an incompressible *interstitial fluid*. Let us assume further that the solid matrix material is incompressible.

Because of the incompressibility condition for both the fluid and the solid matrix the deformation gradient decomposition (3) will be replaced by

$$\mathbf{F}_o \equiv \nabla \chi = \mathbf{F}_\iota \, \mathbf{F}_\phi \,, \tag{55}$$

as shown in the schematic diagram in Fig. 2, where the *porosity distortion*

$$\mathbf{F}_\phi = \beta^{\frac{1}{3}} \, \mathbf{I} \tag{56}$$

describes a spherical porosity growth, while the *elastic distortion* $\mathbf{F}_\iota$ is isochoric

$$\det \mathbf{F}_\iota = 1 \,. \tag{57}$$

Hence the volume change is characterized by

$$\det \mathbf{F}_o = \det \mathbf{F}_\phi = \beta \,. \tag{58}$$

10

In this setting it is customary to measure the amount of matter by its mass, instead of the number of moles. Accordingly, we define the *interstitial fluid content* as the ratio

$$c = \frac{\rho_f}{\rho_o} = \frac{\text{<fluid mass density per unit reference volume>}}{\text{<solid mass density per unit reference volume>}} \, . \tag{59}$$

Denoting by ν_f the *volume per unit mass* of the (incompressible) fluid, the *current volume of fluid per unit reference volume* turns out to be

$$\nu_f \rho_f = \nu_f \rho_o \, c \, . \tag{60}$$

Let us call *porosity* the non-negative scalar field

$$\phi := (\beta - 1) + \phi_o \geq 0 \, , \tag{61}$$

where $(\beta - 1)$ is the *volume increment per unit reference volume*, consisting just of the interstitial volume change because of the solid matrix incompressibility, up to a reference value $0 \leq \phi_o < 1$. The *saturation condition* (the pores are filled with fluid) can then be stated as

$$\phi = \nu_f \rho_f = \alpha \, c \, , \tag{62}$$

where, according to (60),

$$\alpha = \nu_f \rho_o \tag{63}$$

is a positive coefficient independent of time because of *fluid incompressibility*. We make the assumption that the saturation condition holds at any time. Rearranging terms in (61) the other way round we get

$$\beta = 1 + (\phi - \phi_o) = 1 + \alpha \, (c - c_o) \, , \tag{64}$$

with $\phi_o = \alpha \, c_o$, matching definition (5). It is worth noting that, by (64),

$$\dot{\beta} = \dot{\phi} = \alpha \, \dot{c} \, . \tag{65}$$

3.2. Interstitial pressure and interstitial power balance law

In order to state a suitable form of the mass balance law for the interstitial fluid, let us first go back to the species power balance law (15) and define a scalar field $\check{p}$, power conjugate to the interstitial volume rate of change, such that $\forall \mathcal{P}_o \subset \mathcal{R}_o$

$$\int_{\mathcal{P}_o} \mu \rho_o \, \dot{c} \, dV = \int_{\mathcal{P}_o} \check{p} \, \dot{\beta} \, dV \, , \quad \forall \dot{\beta} \, . \tag{66}$$

Localizing we get

$$\mu = \frac{\alpha}{\rho_o} \, \check{p} = \nu_f \, \check{p} \, . \tag{67}$$

Substituting the expression (67) for the chemical potential, we can now consistently transform the species power balance law (15) into

$$\int_{\mathcal{P}_o} \underline{\check{p}} \, \dot{\beta} \, dV = - \int_{\partial \mathcal{P}_o} \underline{\check{p}} \, (\nu_f \, \mathbf{h}_o) \cdot \mathbf{n}_o \, dA + \int_{\mathcal{P}_o} (\nu_f \, \mathbf{h}_o) \cdot \nabla_o \, \underline{\check{p}} \, dV \qquad \forall \underline{\check{p}} \, . \tag{68}$$

If we further define the vector field

$$\mathbf{q}_\mathrm{o} = \nu_f \, \mathbf{h}_\mathrm{o} \,, \tag{69}$$

we finally get the *interstitial power balance law*

$$\int_{\mathcal{P}_\mathrm{o}} \underline{\check{p}} \dot{\beta} \, dV = - \int_{\partial \mathcal{P}_\mathrm{o}} \underline{\check{p}} \, \mathbf{q}_\mathrm{o} \cdot \mathbf{n}_\mathrm{o} \, dA + \int_{\mathcal{P}_\mathrm{o}} \mathbf{q}_\mathrm{o} \cdot \nabla_\mathrm{o} \, \underline{\check{p}} \, dV \qquad \forall \underline{\check{p}} \,. \tag{70}$$

Let us call $\check{p}$ the *interstitial pressure* and $\mathbf{q}_\mathrm{o}$ the *discharge*. It is worth emphasizing that equation (70) still retains its original meaning as the balance law between the amount of matter exchanged through the boundary and the rate of change of its bulk content.

Since we are interested in describing a perfusion in an elastic solid we should again supplement the balance law (70) with the *force power balance law* (19), subject this time to the incompressibility constraint (57).

The reference Piola stress $\mathbf{S}_\mathrm{o}$, the Cauchy stress $\mathbf{T}$ and the intermediate Piola stress $\mathbf{S}$ are now related one another as in (20) with $\mathbf{F}$ replaced by $\mathbf{F}_\iota$

$$\mathbf{S}_\mathrm{o} = (\det \mathbf{F}_\phi) \, \mathbf{T} \, \mathbf{F}_\mathrm{o}^{-\mathsf{T}} = \beta \, \mathbf{T} \, \mathbf{F}_\mathrm{o}^{-\mathsf{T}} = \beta^{\frac{2}{3}} \, \mathbf{T} \, \mathbf{F}_\iota^{-\mathsf{T}} = \beta^{\frac{2}{3}} \, \mathbf{S} \,. \tag{71}$$

3.3. Free energy imbalance

Let us consider for any *constitutive process* the corresponding force power balance

$$\underbrace{\int_{\mathcal{P}_\mathrm{o}} \mathbf{b}_\mathrm{o} \cdot \mathbf{v} \, dV + \int_{\partial \mathcal{P}_\mathrm{o}} \mathbf{t}_\mathrm{o} \cdot \mathbf{v} \, dA}_{\textit{(exchanged) external power}} = \int_{\mathcal{P}_\mathrm{o}} \mathbf{S}_\mathrm{o} \cdot \dot{\mathbf{F}}_\mathrm{o} \, dV \,, \tag{72}$$

together with the interstitial power balance

$$\int_{\mathcal{P}_\mathrm{o}} \check{p} \dot{\beta} \, dV = \underbrace{- \int_{\partial \mathcal{P}_\mathrm{o}} \check{p} \, \mathbf{q}_\mathrm{o} \cdot \mathbf{n}_\mathrm{o} \, dA}_{\textit{(exchanged) external power}} + \int_{\mathcal{P}_\mathrm{o}} \mathbf{q}_\mathrm{o} \cdot \nabla_\mathrm{o} \, \check{p} \, dV \,. \tag{73}$$

Comparing the power exchanged between the matter inside any $\mathcal{P}_\mathrm{o}$ and the outside, with the rate of change of a free energy density per unit reference volume ψ, we get the appropriate form of the *energy imbalance* or *dissipation inequality*

$$\mathbf{S}_\mathrm{o} \cdot \dot{\mathbf{F}}_\mathrm{o} + \check{p} \dot{\beta} - \mathbf{q}_\mathrm{o} \cdot \nabla_\mathrm{o} \, \check{p} - \frac{d}{dt} \psi \geq 0 \,. \tag{74}$$

Because of the decomposition (55) and the relations (64) and (71), the stress power term in (74) takes the expression

$$\mathbf{S}_\mathrm{o} \cdot \dot{\mathbf{F}}_\mathrm{o} = \beta \, \text{dev} \, \mathbf{T} \cdot \dot{\mathbf{F}}_\iota \, \mathbf{F}_\iota^{-1} - p \dot{\beta} \tag{75}$$

where

$$-p \, \mathbf{I} = \text{sph} \, \mathbf{T} \,. \tag{76}$$

It should be emphasized that p is here a *purely reactive pressure* because the elastic distortion is isochoric. A clear picture about this point is given by the species diffusion description of the energy imbalance (52), where the

incompressibility condition $J = 1$ would leave the constitutive characterization of p void, thus qualifying p as reactive.

Replacing (75) into (74) we get the new expression for the *energy imbalance*

$$\beta \ \mathrm{dev}\,\mathbf{T} \cdot \dot{\mathbf{F}}_\iota \, \mathbf{F}_\iota^{-1} + (\check{p} - p)\dot{\beta} - \mathbf{q}_\mathrm{o} \cdot \nabla_\mathrm{o}\,\check{p} - \frac{d}{dt}\psi \geq 0 \,. \tag{77}$$

Guided by (77), we will consider two different choices for the free energy and characterize them by comparing the different evolutions they give rise in a sample problem in sect. 4.

3.4. Type $\mathfrak{g}$ *free energy and constitutive characterization*

Let us consider first a free energy inspired by expression (31)

$$\hat{\psi}^{\mathfrak{g}}(\mathbf{F}_\iota, \beta) = \varphi_\phi(\beta) + \beta\,\varphi_\iota(\mathbf{F}_\iota) \,, \tag{78}$$

which is the sum of a bulk energy density per unit reference volume, dependent on the porosity distortion, and a strain energy density per unit intermediate volume, dependent on the isochoric distortion.

By defining the response functions $\hat{p}_\phi$ and $\hat{\mathbf{S}}^{\mathfrak{g}}$ such that

$$\hat{p}_\phi(\beta)\,\dot{\beta} = \frac{d}{dt}\varphi_\phi(\beta) \,, \tag{79}$$

$$\hat{\mathbf{S}}^{\mathfrak{g}}(\mathbf{F}_\iota) \cdot \dot{\mathbf{F}}_\iota = \frac{d}{dt}\varphi_\iota(\mathbf{F}_\iota) \,, \tag{80}$$

the rate of change of the free energy turns out to be

$$\frac{d}{dt}\hat{\psi}^{\mathfrak{g}}(\mathbf{F}_\iota, \beta) = (\hat{p}_\phi(\beta) + \varphi_\iota(\mathbf{F}_\iota))\dot{\beta} + \beta\,\hat{\mathbf{T}}^{\mathfrak{g}}(\mathbf{F}_\iota) \cdot \dot{\mathbf{F}}_\iota\,\mathbf{F}_\iota^{-1} \,, \tag{81}$$

where by $\hat{\mathbf{T}}^{\mathfrak{g}}(\mathbf{F}_\iota) = \hat{\mathbf{S}}^{\mathfrak{g}}(\mathbf{F}_\iota)\,\mathbf{F}_\iota^\mathsf{T}$ we mean a deviatoric tensor since $\mathrm{tr}\,(\dot{\mathbf{F}}_\iota\,\mathbf{F}_\iota^{-1}) = 0$.

If we substitute (81), into the inequality (77) we finally get

$$\beta\,(\underbrace{\mathrm{dev}\,\mathbf{T} - \hat{\mathbf{T}}^{\mathfrak{g}}(\mathbf{F}_\iota)}_{\mathrm{dev}\,\mathbf{T}^+})) \cdot \dot{\mathbf{F}}_\iota\,\mathbf{F}_\iota^{-1} + (\underbrace{\check{p} - p - (\hat{p}_\phi(\beta) + \varphi_\iota(\mathbf{F}_\iota))}_{\check{p}^+})\dot{\beta} - \mathbf{q}_\mathrm{o} \cdot \nabla_\mathrm{o}\,\check{p} \geq 0 \,, \tag{82}$$

In order for the inequality above to hold for any constitutive process the following conditions must be fulfilled

$$\check{p} = \hat{p}_\phi(\beta) + p + \varphi_\iota(\mathbf{F}_\iota) + \check{p}^+ \,, \quad \check{p}^+\dot{\beta} \geq 0 \,, \tag{83}$$

$$\mathrm{dev}\,\mathbf{T} = \hat{\mathbf{T}}^{\mathfrak{g}}(\mathbf{F}_\iota) + \mathrm{dev}\,\mathbf{T}^+ \,, \quad \mathrm{dev}\,\mathbf{T}^+ \cdot \dot{\mathbf{F}}_\iota\,\mathbf{F}_\iota^{-1} \geq 0 \,, \tag{84}$$

together with

$$-\mathbf{q}_\mathrm{o} \cdot \nabla_\mathrm{o}\,\check{p} \geq 0 \,. \tag{85}$$

Summarizing, from the energy imbalance (77) we get, through (82), the following constitutive characterization of the spherical and deviatoric part of the Cauchy stress

$$\mathrm{sph}\,\mathbf{T} = -(\check{p} - \hat{p}_\phi(\beta) - \varphi_\iota(\mathbf{F}_\iota))\,\mathbf{I} + \mathrm{sph}\,\mathbf{T}^+ \,, \tag{86}$$

$$\mathrm{dev}\,\mathbf{T} = \hat{\mathbf{T}}^{\mathfrak{g}}(\mathbf{F}_\iota) + \mathrm{dev}\,\mathbf{T}^+ \,, \tag{87}$$

13

with $\operatorname{sph} \mathbf{T} = -p \, \mathbf{I}$. We can add them up and get

$$\mathbf{T} = \hat{\mathbf{T}}^{\mathfrak{g}}(\mathbf{F}_\iota) - (\check{p} - \hat{p}_\phi(\beta) - \varphi_\iota(\mathbf{F}_\iota)) \, \mathbf{I} + \mathbf{T}^+ , \tag{88}$$

or, equivalently,

$$\mathbf{T} = \underbrace{\left(\hat{\mathbf{T}}^{\mathfrak{g}}(\mathbf{F}_\iota) + (\hat{p}_\phi(\beta) + \varphi_\iota(\mathbf{F}_\iota)) \mathbf{I} \right)}_{\text{effective stress}} - \check{p} \, \mathbf{I} + \mathbf{T}^+ . \tag{89}$$

By *effective stress* we mean the hyperelastic part of the stress. The *dissipative stress* $\mathbf{T}^+$ can be given any constitutive prescription complying with the inequalities above.

As a final remark notice how (83) describes the coupling between the *interstitial pressure* $\check{p}$ and the *reactive pressure* p, characterizing indeed their difference $(\check{p} - p)$. It is worth noting that $\hat{p}_\phi(\beta)$ is called the *pressure function* in [21], where it is also likened to the chemical potential.

3.5. Type $\mathfrak{s}$ free energy and constitutive characterization

As an alternative, let us consider the simple splitting of the strain energy density per unit reference volume into the sum of a volumetric part and an isochoric part

$$\hat{\psi}^{\mathfrak{s}}(\mathbf{F}_\iota, \beta) = \varphi_\phi(\beta) + \varphi_\iota(\mathbf{F}_\iota) , \tag{90}$$

where $\varphi_\phi(\beta)$ and $\varphi_\iota(\mathbf{F}_\iota)$ are both densities per unit reference volume.

By defining the new response function $\hat{\mathbf{S}}^{\mathfrak{s}}$ such that

$$\beta \left(\hat{\mathbf{S}}^{\mathfrak{s}}(\mathbf{F}_\iota, \beta) \cdot \dot{\mathbf{F}}_\iota \right) = \frac{d}{dt} \varphi_\iota(\mathbf{F}_\iota) , \tag{91}$$

we get the corresponding expression for the rate of change of the free energy

$$\frac{d}{dt} \hat{\psi}^{\mathfrak{s}}(\mathbf{F}_\iota, \beta) = \hat{p}_\phi(\beta) \, \dot{\beta} + \beta \, \hat{\mathbf{T}}^{\mathfrak{s}}(\mathbf{F}_\iota, \beta) \cdot \dot{\mathbf{F}}_\iota \, \mathbf{F}_\iota^{-1} , \tag{92}$$

where again by $\hat{\mathbf{T}}^{\mathfrak{s}}(\mathbf{F}_\iota, \beta)$ we mean just the deviatoric part of $\hat{\mathbf{S}}^{\mathfrak{s}}(\mathbf{F}_\iota, \beta) \, \mathbf{F}_\iota^{\mathsf{T}}$.

If we substitute (92) into the inequality (77) we get

$$\beta \, (\underbrace{\operatorname{dev} \mathbf{T} - \hat{\mathbf{T}}^{\mathfrak{s}}(\mathbf{F}_\iota, \beta)}_{\operatorname{dev} \mathbf{T}^+}) \cdot \dot{\mathbf{F}}_\iota \, \mathbf{F}_\iota^{-1} + (\underbrace{\check{p} - p - \hat{p}_\phi(\beta)}_{\check{p}^+}) \dot{\beta} - \mathbf{q}_{\mathrm{o}} \cdot \nabla_{\mathrm{o}} \, \check{p} \geq 0 , \tag{93}$$

In order for the inequality above to hold for any constitutive process the following conditions must be fulfilled

$$\check{p} = \hat{p}_\phi(\beta) + p + \check{p}^+ , \quad \check{p}^+ \dot{\beta} \geq 0 , \tag{94}$$

$$\operatorname{dev} \mathbf{T} = \hat{\mathbf{T}}^{\mathfrak{s}}(\mathbf{F}_\iota, \beta) + \operatorname{dev} \mathbf{T}^+ , \quad \operatorname{dev} \mathbf{T}^+ \cdot \dot{\mathbf{F}}_\iota \, \mathbf{F}_\iota^{-1} \geq 0 , \tag{95}$$

as well as (85). Summarizing, from the energy imbalance (77) we get, through (93), the following constitutive characterization of the spherical and deviatoric part of the Cauchy stress

$$\operatorname{sph} \mathbf{T} = -(\check{p} - \hat{p}_\phi(\beta)) \, \mathbf{I} + \operatorname{sph} \mathbf{T}^+ , \tag{96}$$

$$\operatorname{dev} \mathbf{T} = \hat{\mathbf{T}}^{\mathfrak{s}}(\mathbf{F}_\iota, \beta) + \operatorname{dev} \mathbf{T}^+ , \tag{97}$$

14

from which we get

$$\mathbf{T} = \hat{\mathbf{T}}^{\mathrm{s}}(\mathbf{F}_\iota, \beta) - (\check{p} - \hat{p}_\phi(\beta))\,\mathbf{I} + \mathbf{T}^+ , \tag{98}$$

or, equivalently,

$$\mathbf{T} = \underbrace{(\hat{\mathbf{T}}^{\mathrm{s}}(\mathbf{F}_\iota, \beta) + \hat{p}_\phi(\beta)\,\mathbf{I})}_{\text{effective stress}} - \check{p}\,\mathbf{I} + \mathbf{T}^+ . \tag{99}$$

The expression for the *effective stress* is consistent with the definition given in [23]. A historical account of this notion development dating back to Terzaghi can be found in [22].

It is worth noting that the two energy terms in (90), differently from (78), turn out not to be coupled anymore by the porosity through β. We will show in sect. 4 the implications of using either $\hat{\psi}^{\mathrm{g}}$ or $\hat{\psi}^{\mathrm{s}}$ through numerical simulations of uniaxial tests.

3.6. Darcy's law

Whatever the free energy expression, condition (85) holds true if

$$\mathbf{q}_{\mathrm{o}} = -\mathbf{K}_{\mathrm{o}}\,\nabla_{\mathrm{o}}\,\check{p} . \tag{100}$$

with $\mathbf{K}_{\mathrm{o}}$ a positive semi-definite tensor. Since, as in (16) and (17),

$$\nabla_{\mathrm{o}}\,\check{p} = \mathbf{F}_{\mathrm{o}}^{\mathsf{T}}\,\nabla\check{p} , \tag{101}$$

$$\mathbf{q}_{\mathrm{o}} = \beta\,\mathbf{F}_{\mathrm{o}}^{-1}\,\mathbf{q} , \tag{102}$$

the expression (100) of *Darcy's law* turns into

$$\mathbf{q} = -\mathbf{K}\,\nabla\check{p} , \tag{103}$$

where the reference and the current *permeability* tensors are related by

$$\mathbf{K}_{\mathrm{o}} = \beta\,\mathbf{F}_{\mathrm{o}}^{-1}\,\mathbf{K}\,\mathbf{F}_{\mathrm{o}}^{-\mathsf{T}} . \tag{104}$$

3.7. Boundary conditions

In order to set up boundary conditions in a consistent way, let us consider a subset $\mathcal{S}_{\mathrm{o}} \subset \partial\mathcal{R}_{\mathrm{o}}$ and the corresponding boundary terms in the *force power balance law* (19) and in the *interstitial power balance law* (70)

$$\int_{\mathcal{S}_{\mathrm{o}}} \mathbf{t}_{\mathrm{o}} \cdot \underline{\mathbf{v}}\,dA , \qquad \int_{\mathcal{S}_{\mathrm{o}}} \underline{\check{p}}\,\mathbf{q}_{\mathrm{o}} \cdot \mathbf{n}_{\mathrm{o}}\,dA , \tag{105}$$

where $\underline{\mathbf{v}}$ is a test velocity field and $\underline{\check{p}}$ is a test interstitial pressure. We should also recall that $\mathbf{q}_{\mathrm{o}}$ is constitutively described by Darcy's law (100).

Let us refer to the usual boundary conditions according to the following table:

$$
\begin{array}{ll}
B_{unc} & \textit{unconstrained boundary deformation} \\
B_{con} & \textit{constrained boundary deformation} \\
B_{perm} & \textit{permeable boundary} \\
B_{imp} & \textit{impermeable boundary}
\end{array}
\tag{106}
$$

15

The boundary terms (105) in the balance laws allow us to characterize explicitly each boundary condition:

B_{unc} the test velocity field $\underline{\mathbf{v}}$ can take any value; thus $\mathbf{t}_o$ should be assigned the value $\mathbf{t}_o^{ext}$ (the external traction), possibly zero;

B_{con} the constraints make the test velocity field $\underline{\mathbf{v}}$ vanish; thus $\mathbf{t}_o$ is just a reactive traction $\mathbf{t}_o^r = \mathbf{S}_o \, \mathbf{n}_o$;

B_{perm} we mean that there is no pressure jump across the boundary, i.e. $\check{p} = p^{ext}$ (the external pressure); hence the test interstitial pressure field $\underline{\check{p}}$ vanishes and $\mathbf{q}_o \cdot \mathbf{n}_o$ is left free;   (107)

B_{imp} we mean that $\mathbf{q}_o \cdot \mathbf{n}_o = 0$ whatever the pressure jump $(\check{p} - p^{ext})$ across the boundary; hence there is no condition on $\check{p}$.

The boundary conditions (107) can also be described on a subset $\mathcal{S} \subset \partial\mathcal{R}$ in terms of the current fields.

Let us examine differently paired boundary conditions on the same subset $\mathcal{S}_o$ or $\mathcal{S}$. To this end it will prove expedient to split the stress constitutive expressions (88) or (98) into a hyperelastic part, the *effective stress*, and the interstitial pressure

$$\mathbf{T} = \hat{\mathbf{T}}^{\text{eff}}(\mathbf{F}_\iota, \beta) - \check{p}\,\mathbf{I}\,. \tag{108}$$

Let us consider first the paired conditions (B_{unc}, B_{perm}). Since $\check{p} = p^{ext}$ the expression for the stress (108) becomes

$$\mathbf{T} = \hat{\mathbf{T}}^{\text{eff}}(\mathbf{F}_\iota, \beta) - p^{ext}\,\mathbf{I}\,. \tag{109}$$

Denoting by $\mathbf{t}^{ext}$ the current traction field on $\mathcal{S}$ and by $\mathbf{n}$ the current unit normal, then

$$\mathbf{T}\,\mathbf{n} = \mathbf{t}^{ext} \quad \Rightarrow \quad \hat{\mathbf{T}}^{\text{eff}}(\mathbf{F}_\iota, \beta)\,\mathbf{n} - p^{ext}\,\mathbf{n} = \mathbf{t}^{ext}\,. \tag{110}$$

Since p^{ext} is a known quantity, we can define $\mathbf{t}^{\text{eff}}$ such that

$$\mathbf{t}^{ext} = \mathbf{t}^{\text{eff}} - p^{ext}\,\mathbf{n}\,. \tag{111}$$

Hence with boundary conditions (B_{unc}, B_{perm}) from (110) we get

$$\hat{\mathbf{T}}^{\text{eff}}(\mathbf{F}_\iota, \beta)\,\mathbf{n} = \mathbf{t}^{\text{eff}}\,. \tag{112}$$

With paired boundary conditions (B_{unc}, B_{imp}), $\check{p}$ and p^{ext} are not related to each other anymore. Thus by (108)

$$\mathbf{T}\,\mathbf{n} = \mathbf{t}^{ext} \quad \Rightarrow \quad \hat{\mathbf{T}}^{\text{eff}}(\mathbf{F}_\iota, \beta)\,\mathbf{n} - \check{p}\,\mathbf{n} = \mathbf{t}^{\text{eff}} - p^{ext}\,\mathbf{n}\,, \tag{113}$$

from which we get

$$\hat{\mathbf{T}}^{\text{eff}}(\mathbf{F}_\iota, \beta)\,\mathbf{n} = \mathbf{t}^{\text{eff}} - (p^{ext} - \check{p})\,\mathbf{n}\,. \tag{114}$$

Let us now consider the paired boundary conditions (B_{con}, B_{perm}). Since $\check{p} = p^{ext}$ the expression (108) will be replaced by (109) and we arrive again at (112) where $\mathbf{t}^{\text{eff}}$ is a *reactive* traction. The paired boundary conditions (B_{con}, B_{imp}) lead again to (114) with $\mathbf{t}^{\text{eff}}$ a *reactive* traction.

16

4. Uniaxial deformation of a poroelastic cylinder

Let us consider a body in the shape of a cylinder undergoing homogeneous uniaxial deformations described by the deformation gradient matrix

$$[\mathbf{F}_\mathrm{o}] = \beta^{\frac{1}{3}} [\mathbf{F}_\iota] = \beta^{\frac{1}{3}} \begin{pmatrix} \lambda & 0 & 0 \\ 0 & \dfrac{1}{\sqrt{\lambda}} & 0 \\ 0 & 0 & \dfrac{1}{\sqrt{\lambda}} \end{pmatrix}, \tag{115}$$

defined in an orthonormal basis $\{\mathbf{e}_1, \mathbf{e}_2, \mathbf{e}_3\}$ with the first basis vector in the axis direction. Let the cylinder be stretched by a couple of opposite axial forces on opposite faces defined by a traction $\mathbf{t} = \tau\,\mathbf{e}_1$, after being submerged in a fluid reservoir at pressure p^{ext}. The cylinder boundary is assumed to be permeable. Hence

$$\check{p} = p^{ext}. \tag{116}$$

From the force balance law we get

$$\mathbf{T} = \mathbf{t} \otimes \mathbf{e}_1 = \tau\,\mathbf{e}_1 \otimes \mathbf{e}_1. \tag{117}$$

Let the energy depending on the porosity distortion be assigned the expression

$$\varphi_\phi(\beta) = k_\phi \left(\beta^2 + \frac{2}{\beta} - 3 \right) \tag{118}$$

which is defined for $\beta > (1 - \phi_\mathrm{o})$, or equivalently for $\phi > 0$, that is in the β range where the material is in the *porous wet phase*, according to (64). Otherwise, when $\phi = 0$ we say that the material is in the *incompressible dry phase*.

Let us consider a neo-Hookean strain energy

$$\varphi_\iota(\mathbf{F}_\iota) = k_\iota\,(\bar{I}_1 - 3), \tag{119}$$

with $\bar{I}_1 = \mathrm{tr}\,(\mathbf{F}_\iota^\mathsf{T}\,\mathbf{F}_\iota)$, to be substituted into both the free energy expressions (78) and (90). The corresponding response functions for the Cauchy stress turn out to be

$$\hat{\mathbf{T}}^\mathrm{g}(\mathbf{F}_\iota) = 2\,k_\iota\,\mathrm{dev}(\mathbf{F}_\iota\,\mathbf{F}_\iota^\mathsf{T}), \tag{120}$$

$$\beta\,\hat{\mathbf{T}}^\mathrm{s}(\mathbf{F}_\iota, \beta) = 2\,k_\iota\,\mathrm{dev}(\mathbf{F}_\iota\,\mathbf{F}_\iota^\mathsf{T}). \tag{121}$$

Further, from (79) and (118) we derive the response function

$$\hat{p}_\phi(\beta) = 2\,k_\phi \left(\beta - \frac{1}{\beta^2} \right), \qquad \beta > (1 - \phi_\mathrm{o}). \tag{122}$$

All of the expressions above can be specialized to the uniaxial deformation gradient (115) by replacing

$$\bar{I}_1 = \lambda^2 + \frac{2}{\lambda}, \tag{123}$$

$$[\mathrm{dev}(\mathbf{F}_\iota\,\mathbf{F}_\iota^\mathsf{T})] = \frac{2}{3}\left(\lambda^2 - \frac{1}{\lambda} \right) \begin{pmatrix} 1 & 0 & 0 \\ 0 & -\dfrac{1}{2} & 0 \\ 0 & 0 & -\dfrac{1}{2} \end{pmatrix}. \tag{124}$$
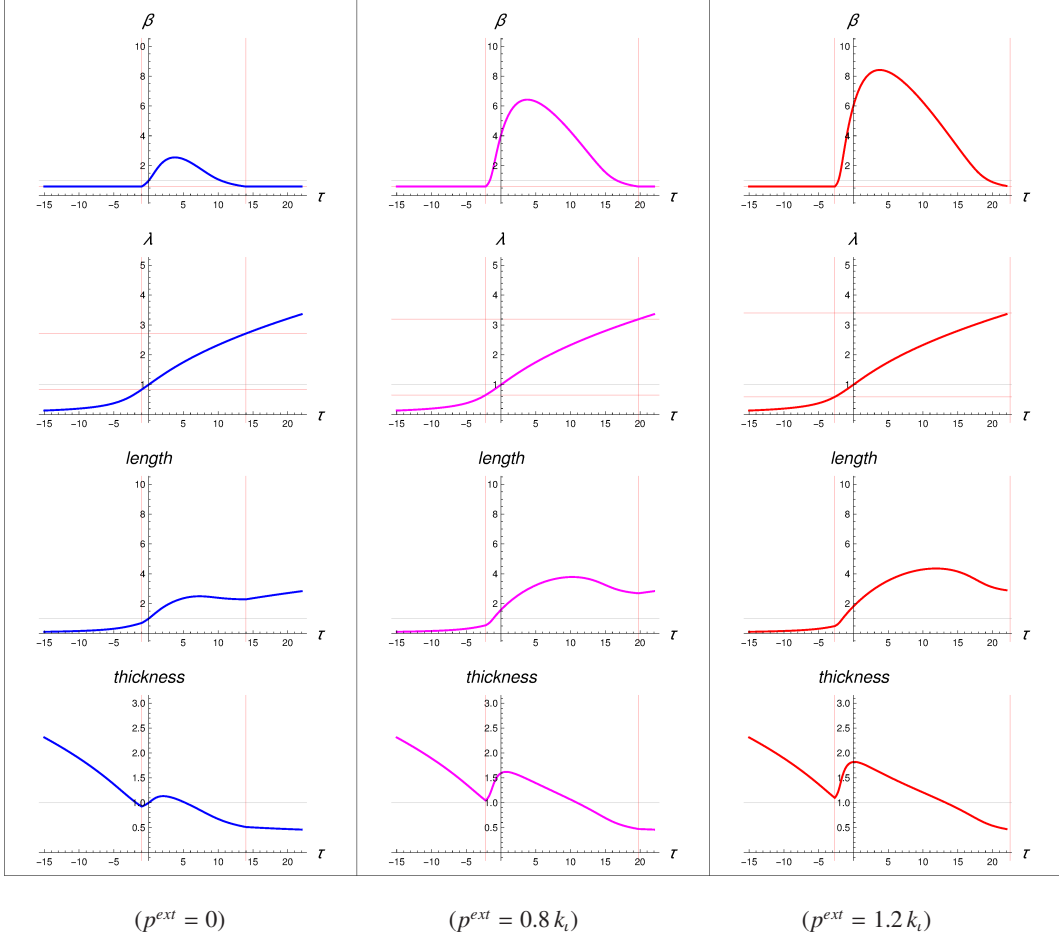
Figure 3: Uniaxial deformation ($\psi^{\mathfrak{g}}$ free energy) with $k_\phi = 0.10\,k_\iota$.

4.1. Type $\mathfrak{g}$ free energy

Substituting the response function (120) into (88) and replacing the stress in the balance equation (117), while neglecting any dissipative term, we get the scalar equations

$$\tau = 2\,k_\iota\left(\lambda^2 - \frac{1}{\lambda}\right), \tag{125}$$

$$p = -\frac{1}{3}\,\tau, \tag{126}$$

$$\check{p} = \hat{p}_\phi(\beta) + p + \varphi_\iota(\mathbf{F}_\iota), \qquad (\phi > 0). \tag{127}$$

In the *incompressible dry phase* ($\phi = 0$) it happens that $\dot\beta$ vanishes making the second term in the dissipation inequality (82) disappear. Hence (127) does not make sense and the resulting relation between λ and β is not defined any more.

Graphs of the solutions to this problem for different values of p^{ext} are arranged in columns in Fig. 3, with

18

$p^{ext} = 0$ on the first column, $p^{ext} = 0.8\,k_\iota$ on the second column, $p^{ext} = 1.2\,k_\iota$ on the third column. Only solutions for $k_\phi = 0.1\,k_\iota$ have been shown. For increasing values of k_ϕ those solutions get closer to the solution for the incompressible dry material, as shown by the graphs in Fig. 4. A thin *horizontal* line marks in every graph in Fig. 3 the unit value of the quantity being plotted against the traction τ, which takes positive values (pulling) or negative values (pushing). The reference porosity has been assigned the value $\phi_o = 0.4$. Correspondingly, a lower thin *horizontal* line in the graphs on the first row marks $\beta = (1 - \phi_o)$, or equivalently $\phi = 0$, the incompressible dry phase. Notice the couple of thin *vertical* lines in each column marking the porous wet phase ($\phi \neq 0$) of the material which is otherwise squeezed to the incompressible dry phase ($\phi = 0$) for τ beyond those limits.

The value of β at $\tau = 0$ is the solution to the equation

$$\check{p} = \hat{p}_\phi(\beta), \tag{128}$$

according to (127). Looking at the first row in Fig. 3 we can notice how, as the traction τ increases, the porosity grows until it reaches a maximum value and then shrinks to zero (marked by the right vertical thin line). That means that after a fluid inflow there is an outflow leading to a dry phase. On the contrary when pushing, the porosity shrinks monotonically until the dry phase is reached (marked by the left thin vertical line). A bit surprising is the way the length and the thickness change when in the porous wet phase, as shown in Fig. 4, where the lower solid thin line is the radial vs axial stretch graph for ($\phi = 0$), while the upper solid thin line is the same graph for ($\phi = \phi_o$).

4.2. Type s free energy

Substituting first the response function (121) into (98) and then replacing the stress in the balance equation (117), we get the scalar equations

$$\tau = 2\,k_\iota \left(\lambda^2 - \frac{1}{\lambda} \right) \frac{1}{\beta}, \tag{129}$$

$$p = -\frac{1}{3}\,\tau, \tag{130}$$

$$\check{p} = \hat{p}_\phi(\beta) + p, \qquad (\phi > 0). \tag{131}$$

The graphs in Fig. 5, describing the corresponding solutions, are arranged the same way as the graphs in Fig. 3. We can notice first how supple this material is when compared to the previous one, and that there is only a thin vertical line separating the porous wet phase (right side) from the incompressible dry phase (left side). That means that when pulling, the porosity grows while the length increases and the thickness decreases. When pushing instead there is a fluid outflow leading soon to a dry phase exhibiting the usual shortening and thickening, as shown also in Fig. 6, where the thin lines are the same graphs as in Fig. 3.
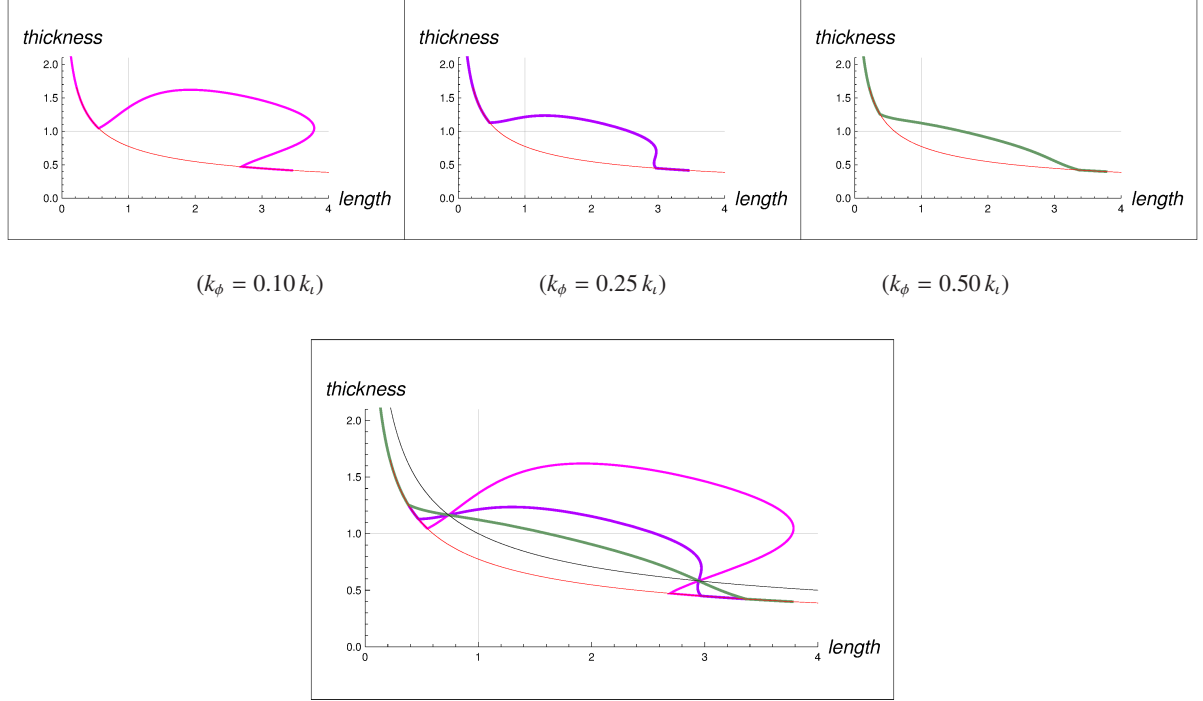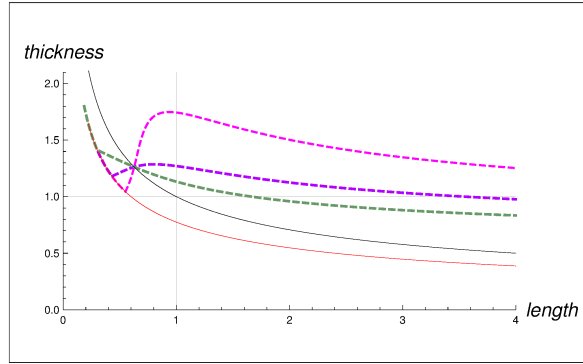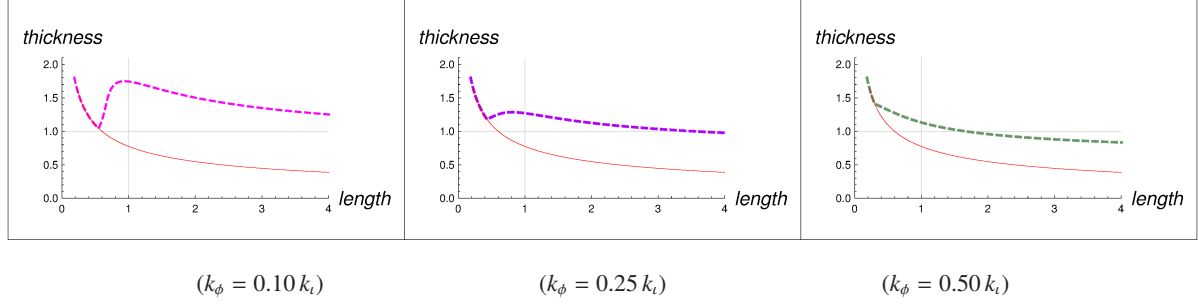
19

Figure 4: Uniaxial deformation ($\psi^{\text{ß}}$ free energy) with $\breve{p} = 0.8 \, k_t$ (lower solid thin line: $\phi = 0$, upper solid thin line: $\phi = \phi_{\text{o}}$).

5. The lamina cribrosa

In the following sections we apply the poroelastic model defined in sect. 3 to study the interplay of blood flow and deformation within the tissue of the LC. However we first need to introduce a constitutive relation linking porosity and permeability, which we do in the next section.

5.1. Permeability constitutive characterization

We derive a microscopic constitutive characterization of the permeability tensor which should be appropriate to the capillary network described by the porosity field. To this end let us consider the capillary network inside a microscopic reference region $\mathcal{P}_m$ and look at the porosity (62) as approximated by the volume ratio

$$\phi = \frac{\pi \, r_c^2 \, L_c}{V_m} \,, \tag{132}$$

where V_m is the $\mathcal{P}_m$ volume, L_c is the total length of the capillary network inside $\mathcal{P}_m$ and r_c is the current value of the capillary radius. Denoting by $L_m = V_m^{1/3}$ a characteristic microscopic length, after defining the *capillary tortuosity* as the constant coefficient

$$t_c := \frac{L_c}{L_m} \,, \tag{133}$$

we get from (132)

$$r_c^2 = \frac{V_m}{\pi \, L_c} \phi = \frac{L_m^2}{\pi \, t_c} \phi \,. \tag{134}$$

20
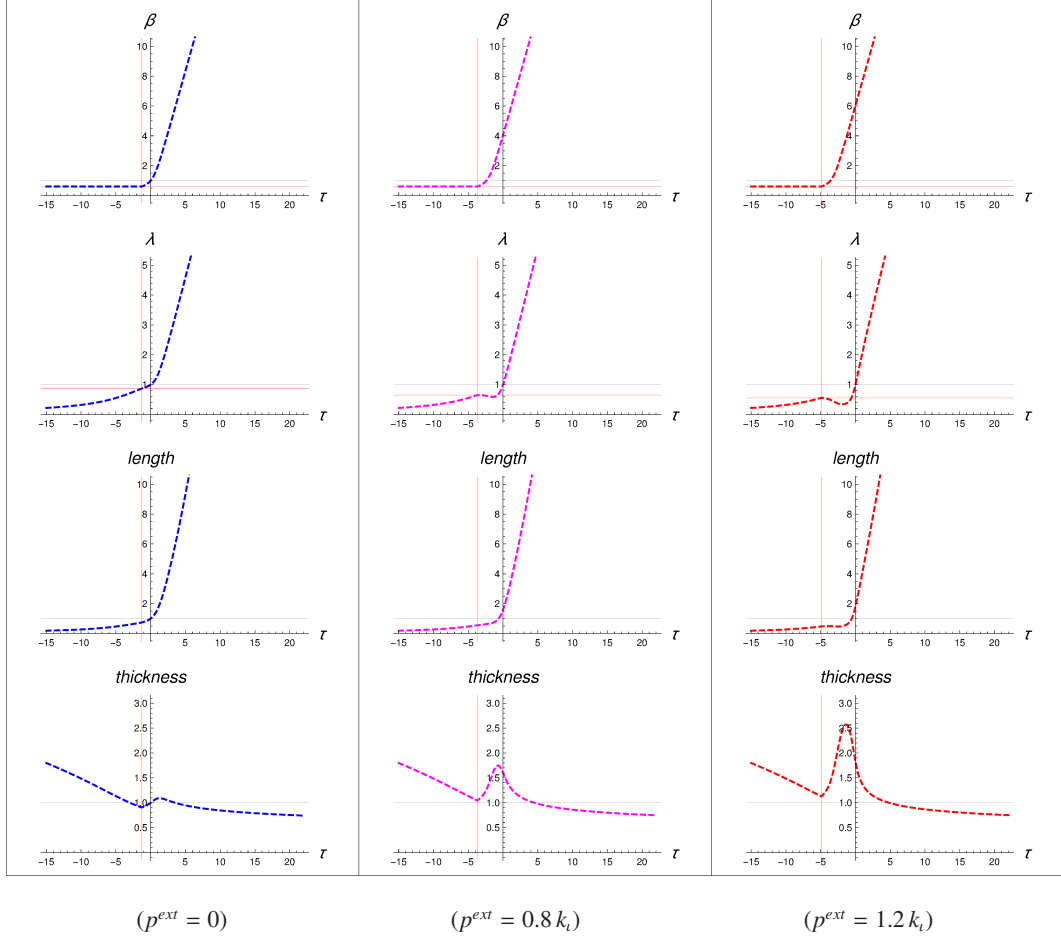
Figure 5: Uniaxial deformation (ψ^5 free energy) with $k_\phi = 0.10\, k_t$.

If we assume that the blood flow in the capillary network is laminar, the volumetric flow rate for a pressure drop Δp_m is given by the Hagen–Poiseuille law

$$Q_m = \frac{\pi\, r_c^4}{8\, \mu_b\, L_c}\, \Delta p_m\, , \tag{135}$$

where μ_b is the blood viscosity. By (133) and (134) this formula turns into

$$Q_m = \frac{L_m^4}{8\, \pi\, \mu_b\, t_c^3}\, \phi^2\, \frac{\Delta p_m}{L_m}\, , \tag{136}$$

from which we get, dividing by a characteristic microscopic area L_m^2 , the discharge

$$q_m = \left(\frac{L_m^2}{8\, \pi\, \mu_b\, t_c^3} \right) \phi^2\, \frac{\Delta p_m}{L_m}\, . \tag{137}$$

If we let a single constant c_g carry the microscopic constitutive description outlined above, then *Darcy's law* (100) takes the special form [12]

$$\mathbf{q} = -\frac{c_g}{\mu_b}\, \phi^2\, \nabla \check{p}\, , \tag{138}$$

21

Figure 6: Uniaxial deformation (ψ^{s} free energy) with $\breve{p} = 0.8\,k_\iota$ (lower solid thin line: $\phi = 0$, upper solid thin line: $\phi = \phi_{\mathrm{o}}$).

showing that the permeability is proportional to the square of the porosity.

As a special case, for the uniaxial deformation in sect. 4 we get through (104) the reference permeability in (100) defined by the scalar expression

$$k_{\mathrm{o}} = \frac{c_g}{\mu_b}\left(\frac{\phi^2}{\lambda^2}\beta^{1/3}\right). \tag{139}$$

Values for the expression between brackets are shown by plots in Fig. 7, consistent with plots in Figs. 3, 5 .
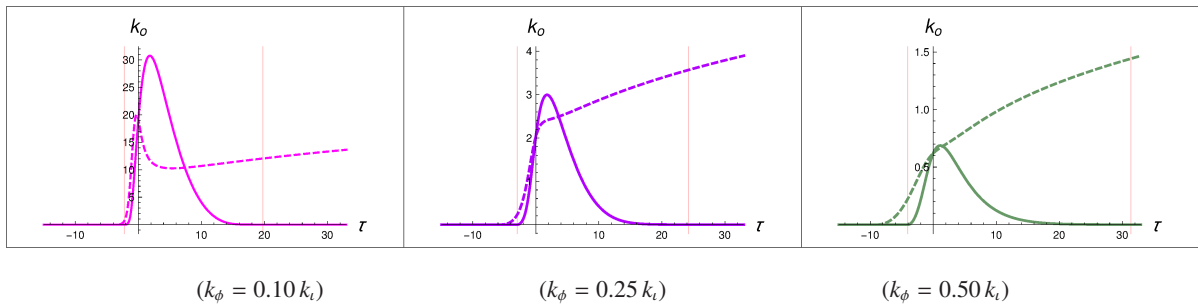
Figure 7: Uniaxial reference permeability with $\breve{p} = 0.8\,k_\iota$ (ψ^{g} solid line, ψ^{s} dashed line).

22

5.2. Numerical simulation setup

Although most works neglect the role played by the surrounding peripapillary sclera when computing the LC deformation, numerical simulations as well as medical imaging [31, 32] show that IOP alterations affect both the LC and the sclera deformations. That is why we considered a fully 3D model of the LC embedded in a sclera spherical cap, pictured in Fig. 8, with physical parameters listed in Table 1.

We used COMSOL Multiphysics® software [33] to carry out our simulations, implementing in their original form:

   i)   the *force power balance law* (19),

   ii)   the *interstitial power balance law* (70),

   iii) *Darcy's law* (100).

We modeled the LC as a poroelastic material with blood as the interstitial fluid, and assumed the material to be characterized, as in sect. 4, by the neo-Hookean strain energy function (119) leading to the response functions (120) and (121), to be substituted in turn into (88) and (98), according to either free energy (78) or (90).

Differently from sect. 4, where condition $\beta > (1 - \phi_{\mathrm{o}})$ was enforced explicitly, the energy depending on the porosity distortion has been given the expression

$$\varphi_\phi(\beta) = k_\phi \, (\beta - 1)^2 \, (\beta - 1 + 3 \, \phi_{\mathrm{o}})/(\beta - 1 + \phi_{\mathrm{o}}) \, , \tag{140}$$

whose value increases to infinity as $\beta \to (1 - \phi_{\mathrm{o}})$, thus preventing the porosity ϕ from reaching a zero value, according to (61). Correspondingly, by (79) we get

$$\hat{p}_\phi(\beta) = 2 \, k_\phi \, (\beta - 1) \, \frac{(\beta - 1)^2 - 3 \, (\beta - 1) \, \phi_{\mathrm{o}} + 3 \, \phi_{\mathrm{o}}^2}{(\beta - 1 + \phi_{\mathrm{o}})^2} \, . \tag{141}$$

The peripapillary sclera has been modeled as a neo-Hookean incompressible non porous solid material.

As boundary conditions we assumed the anterior (facing the vitreous chamber) and the posterior (facing the retrolaminar region) faces of the LC to be impermeable. This means that there is no blood flux through such boundary where we imposed a traction $-p^{ext} \, \mathbf{n}$, with $p^{ext} =$ IOP on the anterior side and $p^{ext} =$ RLTp on the posterior side. We assumed instead the sclera-LC interface, which is the site of the main blood supply to the ONH, to be permeable with external pressure $p^{ext} = P_a$. The central retinal vessel passage, with a fixed radius R_v, has been characterized by a permeable boundary with external pressure $p^{ext} = P_v$. Thus the blood flows through the LC porosity network from the sclera-LC interface to the central retinal vein. The peripapillary sclera outermost boundary was subject to a normal traction corresponding to the mean hoop stress in a spherical vitreous chamber depending on IOP.

5.3. Results

Since we are interested in the interplay between hemodynamics and deformations we mainly focus on porosity and blood flux fields. The LC and peripapillary sclera deformation is shown in the radial cross sections in Figs. 9, 10, 11, with the reference shape in the background, where the porosity field is described by a color map. The sclera
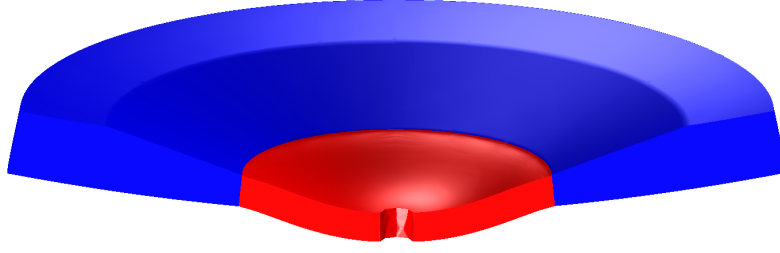
Figure 8: Model LC embedded in the peripapillary sclera.

lamina thickness	$200\,\mu$m
lamina radius	$950\,\mu$m
central retinal vessel passage radius (R_v)	$100\,\mu$m
$\frac{1}{2}$ shear modulus (lamina cribrosa) (k_ι)	$4\,$kPa , $6\,$kPa
$\frac{1}{2}$ bulk modulus (lamina cribrosa) (k_ϕ)	$0.3\,$MPa , $0.5\,$MPa
$\frac{1}{2}$ shear modulus (sclera) (k_ι)	$0.55\,$MPa
reference porosity (ϕ_o)	0.010
Intra Ocular Pressure (IOP)	$15-37\,$mmHg ($2.0-4.9\,$kPa)
Retro Laminar Tissue pressure (RLTp)	$9.75\,$mmHg ($1.3\,$kPa)
ciliary pressure (P_a)	$15\,$mmHg ($2.0\,$kPa)
central vein pressure (P_v)	$7.5\,$mmHg ($1.0\,$kPa)

Table 1: Parameter values used in the simulations.

supports the thinner LC membrane which bends in the anterior-posterior direction under the action of an increasing IOP (from Fig. 9 to Fig. 11), while the RLTp keeps its ground value. The left side and the right side pictures refer respectively to the underlying free energy $\psi^{\mathfrak{g}}$ or $\psi^{\mathfrak{s}}$.

In addition to the maps shown in Figs. 9, 10, 11 we also report in Figs. 12, 13, 14 how some relevant quantities depend on IOP. In particular, in Fig. 12 we plot the anterior-posterior Lamina Cribrosa Displacement (LCD), which is the simplest way of describing the LC cupping, in medical imaging as well as numerical simulations. In the figure LCD is scaled by the lamina thickness and we report its value both for the anterior (thin lines) and the posterior face (thick lines) of the lamina (negative values mean outward displacement). In Fig. 13 we report the mean porosity values scaled by the reference porosity and finally, in Fig. 14, the blood flux through the sclera-LC interface scaled by a typical value. A second set of graphs is shown in Figs. 15, 16, 17 to allow a comparison between the previous results and those obtained with a higher value of the modulus k_ι.

While the deformed shapes exhibited by our LC model in Figs. 9, 10, 11 are close to similar shapes shown in [31, 32], the displayed porosity field carries a more significant information about changes in hemodynamics related to

24

an IOP increase. In this respect a comparison between $\psi^{\mathfrak{g}}$ and $\psi^{\mathfrak{s}}$ free energies is in order. By using the free energy $\psi^{\mathfrak{s}}$ we get some awkward results about porosity and blood flux: looking at the right side pictures in Figs. 9, 10, 11 ($\psi^{\mathfrak{s}}$ free energy), we notice that the porosity increases as the LC cupping proceeds and the thickness becomes smaller and smaller. This is shown clearly by the mean porosity evolution as described by the dashed lines ($\psi^{\mathfrak{s}}$ free energy) in the graphs in Fig. 13. Correspondingly, from the dashed lines in Fig. 14 we notice that the blood flux increases as well, for large enough values of IOP. On the contrary, looking at the solid lines ($\psi^{\mathfrak{g}}$ free energy) in the graphs in Fig. 13, we notice that the mean porosity, after reaching a maximum value, eventually decreases while the corresponding blood flux in Fig. 14 decreases even faster.

This leads us to the conclusion that the $\mathfrak{g}$-type free energy (78) is more suitable to describe the coupling between deformation and porosity than the $\mathfrak{s}$-type free energy (90). The reason for that should be found in the different ways they depend on porosity. It is also interesting to compare the solid line graph in Fig. 13 ($\mathfrak{g}$-type free energy) with the graph in [34, Fig. 5-B], where experimental in-vivo measurements of collagen beam thickness are reported against IOP values. The comparison is meaningful since in our model the porosity network stands for the capillary network running inside the collagen beams, as stated in sect. 1. Both graphs exhibit a maximum value for increasing IOP. This highlights a feature of the $\mathfrak{g}$-type free energy which makes the poroelastic material behave rather differently than the $\mathfrak{s}$-type free energy, as illustrated in sect. 4.

By a closer look at the left side cross sections in Figs. 9, 10, 11 ($\psi^{\mathfrak{g}}$ free energy), we notice the porosity getting lower and lower across the thickness in a region close to the sclera-LC interface. This is reflected in the decreasing blood flux shown by the solid lines in Fig. 14, as opposed to what is shown by the dashed lines. The behavior exhibited by the $\mathfrak{g}$-type free energy could be related to the strong shear deformation localized at the peripheral region of the LC, as shown on the left side of Figs. 18, 19, 20 where, in parallel to the strain energy field on the right side, a color map describes the evolution of the shear strain field defined by

$$\gamma = \frac{\mathbf{a}_r \cdot \mathbf{a}_a}{\|\mathbf{a}_r\| \, \|\mathbf{a}_a\|} \,, \quad \text{with} \quad \mathbf{a}_r = \mathbf{F}_o \, \mathbf{e}_r \,, \ \mathbf{a}_a = \mathbf{F}_o \, \mathbf{e}_a \,, \tag{142}$$

denoting by $\mathbf{e}_a$ and $\mathbf{e}_r$ an axial (parallel to the eye axis) and a radial (toward the center of the LC) reference orthonormal vectors. This turns out to be consistent with the onset and progression of the loss of vision related to glaucoma: the peripheral vision deteriorates, and eventually is lost altogether, as the visual field shrinks to a small region in the center of the eye [3], [32].

We look at the above description of the mechanism leading to a blood flow reduction as the main result from our numerical simulations.
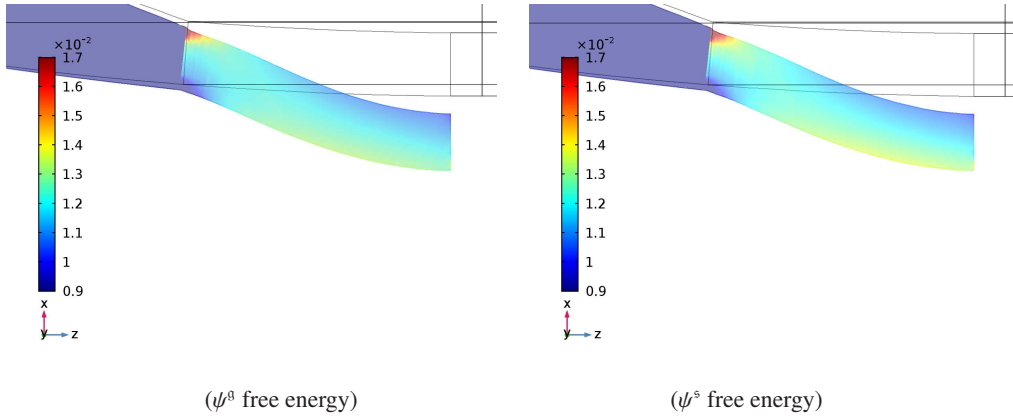
(ψ^{g} free energy)   (ψ^{s} free energy)

Figure 9: Porosity field ϕ/ϕ_{o} on a deformed shape cross section for IOP = 15 mmHg (with k_{ϕ} = 0.3 MPa and k_t = 4 kPa).
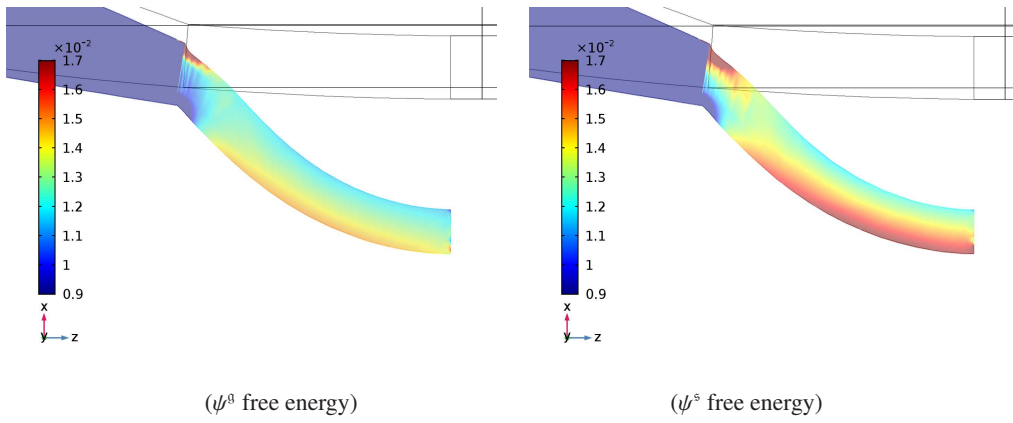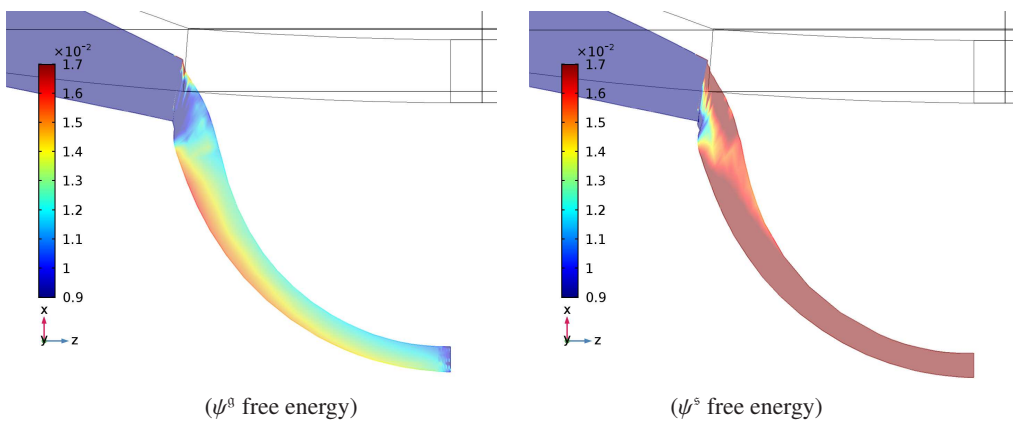

(ψ^{g} free energy)   (ψ^{s} free energy)

Figure 10: Porosity field ϕ/ϕ_{o} on a deformed shape cross section for IOP = 25 mmHg (with k_{ϕ} = 0.3 MPa and k_t = 4 kPa).

(ψ^{g} free energy)   (ψ^{s} free energy)

Figure 11: Porosity ϕ/ϕ_{o} on a deformed shape cross section for IOP = 35 mmHg (with k_{ϕ} = 0.3 MPa and k_t = 4 kPa).
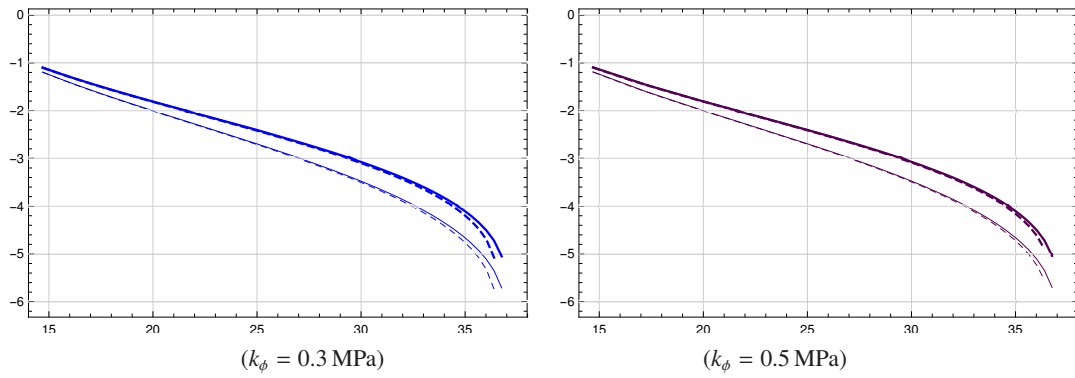
Figure 12: Scaled anterior-posterior LCD vs IOP (ψ^g solid line, ψ^s dashed line; thin lines refer to the inner face) with $k_\iota = 4$ kPa.
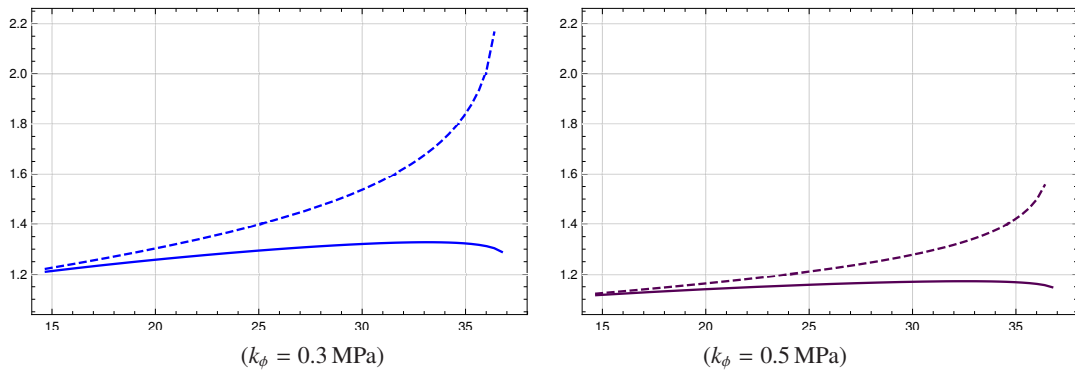
Figure 13: Scaled mean porosity vs IOP (ψ^g solid line, ψ^s dashed line) with $k_\iota = 4$ kPa.
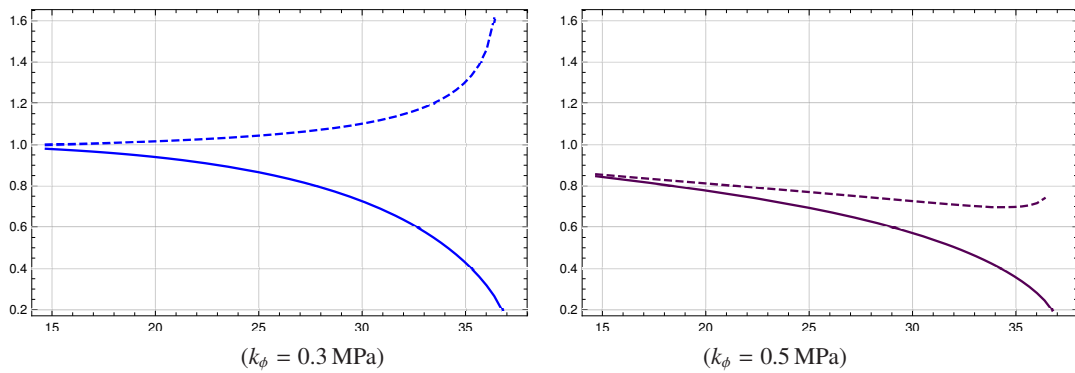
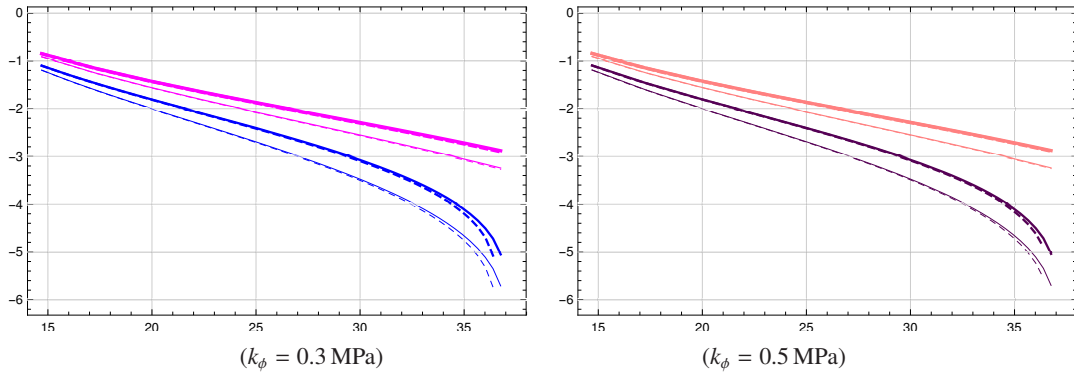Figure 14: Scaled boundary flux vs IOP (ψ^g solid line, ψ^s dashed line) with $k_\iota = 4$ kPa.

Figure 15: Scaled anterior-posterior LCD vs IOP ($\psi^{\mathfrak{g}}$ solid line, $\psi^{\mathfrak{s}}$ dashed line) with $k_t = 4\,\text{kPa}$ and $k_t = 6\,\text{kPa}$ (thick line).
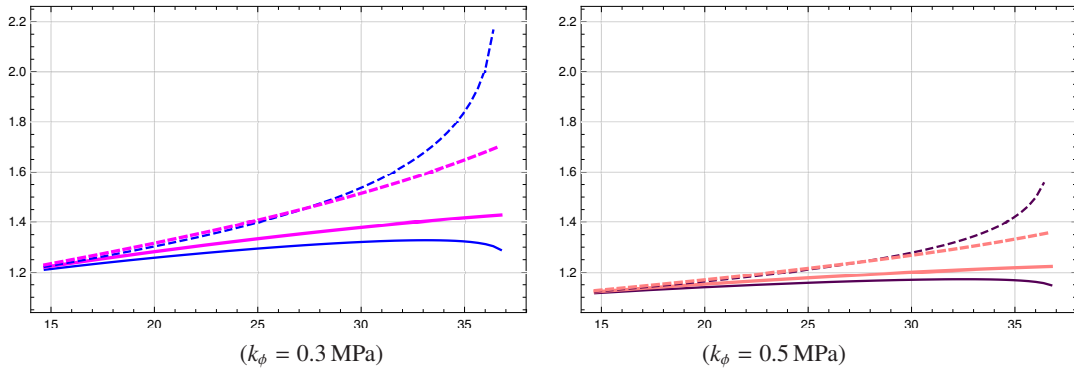
Figure 16: Scaled mean porosity vs IOP ($\psi^{\mathfrak{g}}$ solid line, $\psi^{\mathfrak{s}}$ dashed line) with $k_t = 4\,\text{kPa}$ and $k_t = 6\,\text{kPa}$ (thick line).
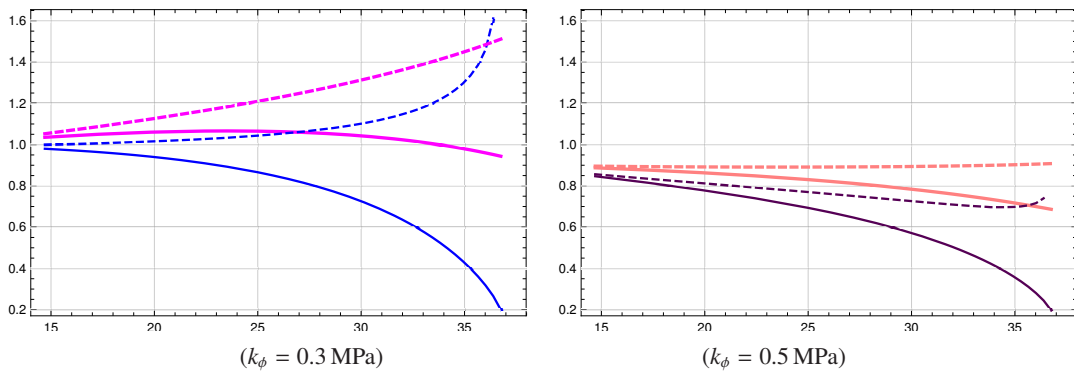
Figure 17: Scaled boundary flux vs IOP ($\psi^{\mathfrak{g}}$ free energy) with $k_t = 4\,\text{kPa}$ and $k_t = 6\,\text{kPa}$ (thick line).

28
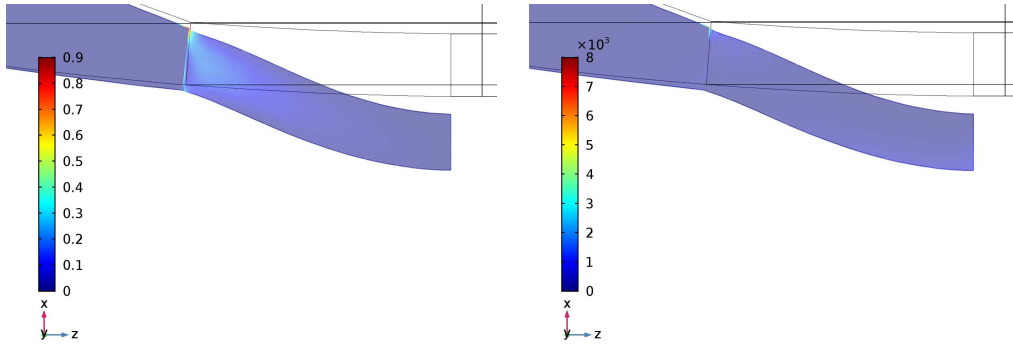
Figure 18: Shear strain (left) and strain energy density (right) for IOP = 15 mmHg (ψ^{g} free energy with k_ϕ = 0.3 MPa and k_t = 4 kPa).
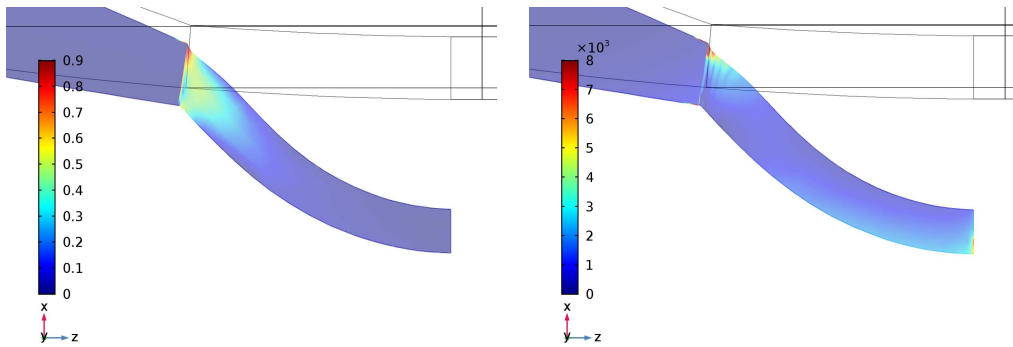

Figure 19: Shear strain (left) and strain energy density (right) for IOP = 25 mmHg (ψ^{g} free energy with k_ϕ = 0.3 MPa and k_t = 4 kPa).
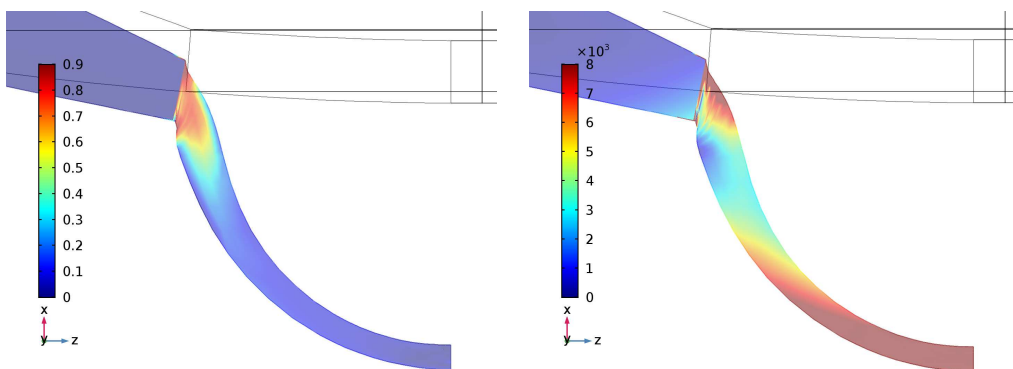

Figure 20: Shear strain (left) and strain energy density (right) for IOP = 35 mmHg (ψ^{g} free energy with k_ϕ = 0.3 MPa and k_t = 4 kPa).

29

6. Conclusions

An increased IOP can lead to a significant blood flow reduction in the LC.

The g-type free energy describes much better than the s-type free energy the coupling between deformation and porosity. That coupling, endowed in the free energy expression, is carried separately by a porosity dependent permeability. Modeling in parallel species diffusion and fluid perfusion emphasizes how the two mechanical models can be cast in the same framework (balance laws and dissipation inequality). The common framework helps also to better grasp the relation between chemical potential and interstitial pressure and the origin of their constitutive characterization.

The structurally weak LC deforms under a raising IOP, showing a noticeable shear deformation on the boundary, together with a deep cupping. Our simulation outcome strongly correlates the shear deformation to porosity and blood flux decrease. Because the main blood supply to the optic nerve head is from the posterior ciliary artery via the peripapillary choroid and the circle of Zinn-Haller, the blood flux reduction on the LC boundary results in an alteration of the blood supply to the optic nerve head.

As a concluding remark we observe that the LC model could be enriched by anisotropic properties of the intricate framework of collagen beams carrying the capillary network while supporting the axons [11], and even by a remodeling mechanism triggered by the high shear strain on the boundary [35, 36]. Further, the axons themselves could enter the model as an additional network allowing to couple both axonal transport and blood perfusion with LC deformation and stress [2]. Nevertheless our essential description of a poroelastic model has proven useful to account for the interplay between LC deformation and hemodynamics in the glaucoma pathophysiology.

References

[1] National Eye Institute.
    URL https://nei.nih.gov/health/glaucoma/

[2] C. Burgoyne, A biomechanical paradigm for axonal insult within the optic nerve head, Exp. Eye Res. 93 (2011) 120–132. doi:10.1016/j.exer.2010.09.005.

[3] N. N. Osborne, J. Melena, G. Chidlow, J. P. M. Wood, A hypothesis to explain ganglion cell death caused by vascular insults at the optic nerve head: possible implication for the treatment of glaucoma, Br. J. Ophthalm. 85 (2001) 1252–1259. doi:10.1136/bjo.85.10.1252.

[4] I. A. Sigal, C. R. Ethier, Biomechanics of the optic nerve head, Exp. Eye Res. 88 (4) (2009) 799–807.

[5] C. F. Burgoyne, J. C. Downs, A. J. Bellezza, J.-K. F. Suh, R. T. Hart, The optic nerve head as a biomechanical structure: a new paradigm for understanding the role of IOP-related stress and strain in the pathophysiology of glaucomatous optic nerve head damage, Progress in retinal and eye research 24 (1) (2005) 39–73.

[6] G. Guidoboni, A. Harris, L. Carichino, Y. Arieli, B. A. Siesky, Effect of intraocular pressure on the hemodynamics of the central retinal artery: A mathematical model, Math. Biosci. Eng. 11 (2014) 523–546. doi:10.3934/mbe.2014.11.523.

[7] A. Harris, G. Guidoboni, J. C. Arciero, A. Amireskandari, L. A. Tobe, B. A. Siesky, Ocular hemodynamics and Glaucoma: The role of mathematical modeling, Eur. J. Ophthalmol. 23 (2013) 139–146. doi:10.5301/ejo.5000255.

[8] J. C. Downs, Optic nerve head biomechanics in aging and disease, Exp. Eye Res. 133 (2015) 19–29. doi:10.1016/j.exer.2015.02.011.

[9] R. N. Weinreb, A. Harris (Eds.), Ocular Blood Flow in Glaucoma, Kugler Publications, 2009.
URL https://www.kuglerpublications.com/index.php?p=274&page=publication

[10] I. A. Sigal, M. D. Roberts, M. J. A. Girard, C. F. Burgoyne, J. C. Downs, Chapter 20–Biomechanical changes of the optic disc, in: L. A. Levin, D. M. Albert (Eds.), Ocular Disease, W.B. Saunders, Edinburgh, 2010, pp. 153–164. doi:10.1016/B978-0-7020-2983-7.00020-6.

[11] T. Chuangsuwanich, K. E. Birgersson, A. Thiery, S. G. Thakku, H. L. Leo, M. J. A. Girard, Factors influencing lamina cribrosa microcapillary hemodynamics and oxygen concentrations., Invest. Ophthalmol. Vis. Sci. 57 (2016) 6167–6179. doi:10.1167/iovs.16-20167.

[12] P. Causin, G. Guidoboni, A. Harris, D. Prada, R. Sacco, S. Terragni, A poroelastic model for the perfusion of the lamina cribrosa in the optic nerve head, Math. Biosci. 257 (2014) 33–41. doi:10.1016/j.mbs.2014.08.002.

[13] A. F. Bower, P. R. Guduru, V. A. Sethuraman, A finite strain model of stress, diffusion, plastic flow, and electrochemical reactions in a lithium-ion half-cell, J. Mech. Phys. Solids 59 (2011) 804–828. doi:10.1016/j.jmps.2011.01.003.

[14] Z. W. Cui, F. Gao, J. M. Qu, A finite deformation stress-dependent chemical potential and its applications to lithium ion batteries, J. Mech. Phys. Solids 60 (2012) 1280–1295. doi:10.1016/j.jmps.2012.03.008.

[15] C. V. Di Leo, E. Rejovitzky, L. Anand, A Cahn–Hilliard-type phase-field theory for species diffusion coupled with large elastic deformations, J. Mech. Phys. Solids 70 (2014) 1–29. doi:10.1016/j.jmps.2014.05.001.

[16] M. E. Gurtin, E. Fried, L. Anand, The Mechanics and Thermodynamics of Continua, Cambridge University Press, 2010.

[17] F. Larché, J. W. Cahn, The interactions of composition and stress in crystalline solids, J. of Research of the National Bureau of Standards 89 (1984) 467–500.

[18] B. D. Coleman, W. Noll, The thermodynamics of elastic materials with heat conduction and viscosity, Arch. Rational. Mech. Anal. 13 (1963) 167–178.

[19] C. H. Wu, The role of Eshelby stress in composition-generated and stress-assisted diffusion, J. Mech. Phys. Solids 49 (2001) 1771–1794.

[20] J. D. Eshelby, Elastic energy-momentum tensor, J. Elasticity 5 (1975) 321–335. doi:10.1007/BF00126994.

[21] M. A. Biot, Theory of finite deformations of porous solids, Indiana University Mathematics Journal 21 (7) (1972) 597–620.
URL http://www.jstor.org/stable/24890361

[22] R. de Boer, Theory of porous media, Springer, 2000. doi:10.1007/978-3-642-59637-7.

[23] O. Coussy, Poromechanics, John Wiley & Sons, 2004.

[24] G. A. Ateshian, On the theory of reactive mixtures for modeling biological growth, Biomechan. Model. Mechanobiol. 6 (2007) 423–445. doi:10.1007/s10237-006-0070-x.

[25] D. Chapelle, P. Moireau, General coupling of porous flows and hyperelastic formulations – From thermodynamics principles to energy balance and compatible time schemes, Eur. J. Mech. B/Fluids 46 (2014) 82–96. doi:10.1016/j.euromechflu.2014.02.009.

[26] C. W. MacMinn, E. R. Dufresne, J. S. Wettlaufer, Large deformations of a soft porous material, Phys. Rev. Applied 5 (2016) 044020. doi:10.1103/PhysRevApplied.5.044020.

[27] W. Hong, X. Zhao, J. Zhou, Z. Suo, A theory of coupled diffusion and large deformation in polymeric gels, J. Mech. Phys. Solids 56 (2008) 1779–1793. doi:10.1016/j.jmps.2007.11.010.

[28] M. Doi, Gel dynamics, Journal of the Physical Society of Japan 78 (2009) 052001–1–052001–19. doi:10.1143/JPSJ.78.052001.

[29] F. P. Duda, A. C. Souza, E. Fried, A theory for species migration in a finitely strained solid with application to polymer network swelling, J. Mech. Phys. Solids 58 (2010) 515–529. doi:10.1016/j.jmps.2010.01.009.

[30] W. J. Vankan, J. M. Huyghe, J. D. Janssen, A. Huson, Poroelasticity of saturated solids with an application to blood perfusion, Int. J. Engng. Sci. 34 (1996) 1019–1031. doi:10.1016/0020-7225(96)00009-2.

[31] I. A. Sigal, H. Yang, M. D. Roberts, C. F. Burgoyne, J. C. Downs, IOP-induced lamina cribrosa displacement and scleral canal expansion: An analysis of factor interactions using parameterized eye-specific models, Invest. Ophthalmol. Vis. Sci. 52 (2011) 1896–1907. `doi:10.1167/iovs.10-5500`.

[32] C. Burgoyne, The morphological difference between glaucoma and other optic neuropathies, J. Neuroophthalmol. 35 (2015) S8–S21. `doi:10.1097/WNO.0000000000000289`.

[33] COMSOL Multiphysics® Reference Manual, version 5.3. URL `https://www.comsol.com`

[34] B. Wang, H. Tran, M. A. Smith, T. Kostanyan, S. E. Schmitt, R. A. Bilonick, N.-J. Jan, L. Kagemann, E. C. Tyler-Kabara, H. Ishikawa, J. S. Schuman, I. A. Sigal, G. Wollstein, In-vivo effects of intraocular and intracranial pressures on the lamina cribrosa microstructure, PLoS ONE 12 (2017) (11): e0188302. `doi:10.1371/journal.pone.0188302`.

[35] J. C. Downs, M. D. Roberts, I. A. Sigal, Glaucomatous cupping of the lamina cribrosa: A review of the evidence for active progressive remodeling as a mechanism, Exp. Eye Res. 93 (2011) 133–140. `doi:10.1016/j.exer.2010.08.004`.

[36] R. Grytz, G. Meschke, J. B. Jonas, The collagen fibril architecture in the lamina cribrosa and peripapillary sclera predicted by a computational remodeling approach, Biomech. Model. Mechanobiol. 10 (2011) 371–382. `doi:10.1007/s10237-010-0240-8`.